The Institute of Paper Science and Technology

Atlanta, Georgia

Doctor's Dissertation

A Study of Fume Particle Deposition

Kristin A. Goerg

May, 1989

A STUDY OF FUME PARTICLE DEPOSITION

A thesis submitted by

Kristin A. Goerg

B. S. ChE., May 1984, University of Wisconsin, Madison
M. S., June 1986, The Institute of Paper Chemistry

in partial fulfillment of the requirements
of The Institute of Paper Chemistry
for the degree of Doctor of Philosophy
from Lawrence University
Appleton, Wisconsin

May, 1989

TABLE OF CONTENTS

ABSTRACT

Mechanisms responsible for fume deposition on kraft recovery furnaces were studied. The main reason for determining the mechanisms is to understand the controlling parameters, thereby obtaining the ability to affect the deposition rate by changing these parameters. The following mechanisms were reviewed and examined as possible fume deposition mechanisms: molecular diffusion, Brownian motion, turbulent diffusion, particle impaction, thermophoresis, and vapor diffusion/crystallization.

Thermophoresis was found to be the main deposition mechanism for fume particles under the following experimental conditions:

1. Fume particle sizes from 0.1 μm to 1 μm in diameter.

2. Flue gas temperatures from 250°C to 580°C.

3. Reynolds numbers less than 3 (based on cooled tube diameter).

The following equation was derived:

$$\text{Dep. rate (g/min/cm}^2) = 0.036 \, \alpha_T \, d_p \, C \left(\frac{T_c - T_w}{T_w} \right)$$

where:

α_T = thermal diffusion factor, dimensionless

d_p = particle diameter, μm

C = fume concentration in flue gas, g/L

T_c = bulk flue gas temperature, absolute

T_w = tube surface temperature, absolute

This equation applies to Na_2CO_3, Na_2SO_4, NaCl, and simultaneous Na_2SO_4/NaCl fume deposition and is similar in form to thermophoretic equations derived by other authors.

These results are directly applicable to fume deposition in the generating bank and the economizer section in recovery boilers, where flue gas temperatures range from 200°C to 700°C. The Reynolds number in a boiler bank is between 3000 and 5000; the heat transfer coefficient is a function of Reynolds number and the deposition rate is proportional to the heat transfer coefficient. If the difference in flow rate between the experimental system and the recovery boiler is taken into account, the experimental results show close agreement with actual recovery boiler data.

The presence of water vapor in the incoming gas streams to the reactor affected the fume composition; fume contained less Na_2CO_3 and more Na_2SO_4 when water vapor was present during fume formation.

INTRODUCTION

One of the products of black liquor combustion is fume. Fume consists of very small particles, approximately 0.25 μm to 1 μm in diameter; it is mainly composed of sodium sulfate, sodium carbonate, sodium chloride, and potassium salts.

Chemical fume formation is of interest because fume is partly responsible for the fireside deposits formed on the cooled surfaces in the superheater section, generating banks, and economizer region of the recovery boiler. These deposits provide an additional resistance to heat transfer, which then affects the heat transfer rate between the flue gas outside the tubes and the steam inside the tubes. Fume plugs gas passages and therefore influences the gas flow rate and flow resistance. Fume and other deposits on recovery boiler surfaces may accelerate corrosion. Fume in the upper sections of a recovery boiler is also enriched in chloride and potassium which lower the sticky temperature of the fume and increase the hardness of the deposit. Na_2CO_3 fume, however, does have the advantage of reacting with sulfur gases and thereby forming sulfur-containing particles that are collected by the precipitator.

Because fume deposits have various detrimental effects on the recovery boiler and its operation, the paper industry would benefit from knowledge concerning the mechanisms responsible for deposition and these mechanisms' controlling parameters. Recovery boiler operators would then have the ability to change the deposition rate by varying these parameters. Conversely, it may be determined that changing the controlling parameters for fume deposition would not be beneficial to recovery boiler operation as a whole.

RECOVERY BOILER CONDITIONS

In order to determine the possible mechanisms for fume deposition in a recovery boiler, boiler conditions must be known. Average values of these conditions were obtained from an actual recovery boiler[1]. According to this data, the tubes in the boiler bank are 2 1/2" in diameter (on the average); they vary between 2" and 3" in diameter. There is a 4 3/4" spacing between the tubes.

Gas temperatures in the mid-section of the boiler bank range from an incoming temperature of 700°C to an outgoing temperature of 430°C. Average temperatures in the economizer section are between 200°C and 400°C. Gas velocities in the boiler bank are approximately 20 ft/sec, which corresponds to a Reynolds number of 4800 at a temperature of 540°C. The Reynolds number in this region of the boiler varies from 3000 to 5000. For fluids flowing normal to a bank of cylindrical tubes, Re<100 is considered laminar flow. Fully developed turbulent flow does not exist until Re>10,000; the transition region therefore covers a wide range of Reynolds numbers - 100<Re<10,000. Flue gas flowing in the boiler bank is in this transition region.

RECOVERY BOILER FUME

Fume has a high specific surface area due to its submicron size. This makes it very reactive in the flue gas; most of its alkali compounds are converted to sulfates. The chemical composition of fume in the generating banks, economizer, and precipitator is influenced by sulfidity, the chemical composition of the black liquor, and the bed temperature.

Higher bed temperatures result in more Na_2CO_3 fume formation and less sulfur in the flue gas. This in turn decreases the Na_2SO_4 content of the fume[2]. High bed temperatures also cause more chloride and potassium salts to vaporize from the

smelt, which enriches the fume with these compounds. Lower sulfidity liquor produces less sulfur gases[3]; this results in a lower Na_2SO_4 content in the fume.

Reeve et. al.[4,5], Tran et. al.[6,7,8,9], and Isaak[10] have obtained data from deposits in a recovery boiler. They have defined two mechanisms by which deposits can form:

1. "Carryover" - smelt and/or partially burned black liquor particles physically entrained in the flue gas.
2. "Condensation" - fume forming either by condensation directly on cooled surfaces, or indirectly in the flue gas stream (these particles are then transferred to the cool surfaces).

These authors inserted a probe into the furnace and found that in the lower superheater, carryover is dominant. Deposits on the upstream side were black, hard, and thick and consisted mostly of black liquor particles that were entrained in the flue gas. Deposits on the downstream side were white and thinner, which the authors assumed to be fume deposits.

Deposition at higher elevations in the superheaters was slightly different. A layer of white powder, which became thicker with time, was formed on both the upstream and downstream side of the probe. The deposit thickness was greater on the upstream side than on the downstream side.

No deposition data was obtained by probe insertion into the upper regions of the recovery furnace, such as in the generating bank, economizer region, and precipitator. However, the chemical composition of the deposits in these sections has been determined. Tran[3] found that the chemical composition of the deposits in the boiler bank, economizer, and precipitator are very similar to each other, but different from the composition of superheater deposits. Superheater deposits

consisted of approximately 2% carbon, 45% Na_2SO_4, 47% Na_2CO_3, and 6% chloride and potassium salts. Deposits in the upper boiler sections consisted of 80% Na_2SO_4, 5% Na_2CO_3, and 15% chloride and potassium salts. This shows that deposits in the generating bank, economizer, and precipitator are enriched in chloride and potassium and depleted in Na_2CO_3, which is indicative of fume particles and not carryover particles. Fume, therefore, is the major constituent of deposits in these areas.

Bosch et. al.[11] have measured particle size distributions in the electrostatic precipitator. They found particle sizes ranging from less than 0.6 μm to greater than 20 μm. Most of the particles were smaller than 1.4 μm, with 50% of the collected weight being composed of particles under 1 μm. Particles at the precipitator outlet were smaller than at the precipitator inlet.

The authors contributed the wide particle size range to two independent aerosols being collected: carryover and fume. Carryover particles were assumed to be the larger particles, but the authors did not state what the carryover particle size range was. No data were obtained for particle size distributions in the generating bank and economizer. The fume particle sizes in these regions may be different than in the precipitator.

Na_2CO_3, Na_2SO_4, NaCl fume, and combinations thereof can all be generated under ideal conditions on a laboratory scale. The fume composition in the laboratory can be controlled and varied; however, the fume particle size is, with current knowledge, impossible to vary. Laboratory fume particles, therefore, may not be the same size as that found in upper sections of the recovery boiler. The laboratory fume particle size, for a given fume composition, is constant; experiments, therefore, at least yield consistent results in terms of particle size.

SODIUM CARBONATE FUME

Na$_2$CO$_3$ fume generation occurs when sodium sulfide in a Na$_2$S/Na$_2$CO$_3$ melt is oxidized by air[2,12,13]; sodium carbonate fume is then produced. Recent work at The Institute of Paper Chemistry[2,12] has shown that Na$_2$CO$_3$ fume is formed by a liquid phase reaction followed by a gas phase reaction:

$$4\,Na_2CO_3 + Na_2S \longleftrightarrow Na_2SO_4 + 4\,CO_2 + 8\,Na \tag{1}$$

$$2\,O_2 + 4\,CO_2 + 8\,Na \longleftrightarrow 4\,Na_2CO_3 \tag{2}$$

All equations in this thesis are stoichiometric equations which do not necessarily describe the reaction mechanisms.

SODIUM SULFATE FUME

In a recovery boiler, typical fume deposits consist mostly of Na$_2$SO$_4$, some chloride and potassium salts, and only a small amount of sodium carbonate[3]. Tran[3] has shown that the Na$_2$CO$_3$/Na$_2$SO$_4$ ratio in deposits decreased as the gases traveled up the furnace. Tran also states that Na$_2$CO$_3$ can react with SO$_2$ and O$_2$ to form sodium sulfate by the following reaction[2]:

$$2\,Na_2CO_3 + 2\,SO_2 + O_2 \longrightarrow 2\,Na_2SO_4 + 2CO_2 \tag{3}$$
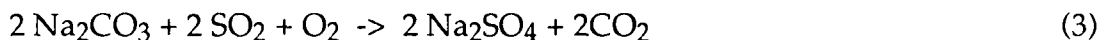
These results indicate that, in a recovery boiler, sulfate fume may be formed from the reaction of sodium carbonate, sulfur dioxide, and oxygen.

SODIUM CHLORIDE FUME

NaCl fume is formed by the vaporization of NaCl from the smelt bed. If vaporization of sodium chloride is an equilibrium controlled process, the vaporization rate may be calculated using Raoult's law and assuming that the gas

stream is saturated in NaCl. Raoult's law states (see Appendix I for symbol definitions)[14]:

$$p_{NaCl(T)} = p^*_{NaCl(T)} X_{NaCl} \qquad (4)$$

The vaporization rate, hence the NaCl fume generation rate, can then be calculated by the following equation:

$$\text{vaporization rate} = \text{molar gas flow rate} * p_{NaCl(T)} \qquad (5)$$

At 950ºC, the vapor pressure of pure NaCl is approximately 4.5 mm Hg.

PARTICLE DEPOSITION MECHANISMS

There are six principal mechanisms by which particles can be deposited from a high temperature gas stream to a cooler surface[15,16]. These mechanisms are functions of the gas flow and the particle size. They are:

1. Molecular diffusion.

2. Brownian motion.

3. Turbulent diffusion.

4. Particle impaction.

5. Thermophoresis.

6. Vapor diffusion/crystallization.

Flow conditions near the deposition surface are different from those in the bulk of the moving gas; boundary layers may be laminar while bulk flow is turbulent. These flow conditions affect the motion of particles approaching the surface and therefore affect the rate of deposition as well as change the mechanism of deposition.

On cylindrical surfaces immersed at right angles to the flowing gas, the thickness of the boundary layer is less on the upstream side and more on the downstream side[17], as shown in Fig. 1. The thickness of the boundary layer, which is dependent on such variables as the gas velocity and the cylinder diameter, is an important parameter in the rate of deposition. The mechanism of deposition may also be determined by the pattern of the boundary layer, because different mechanisms are dominant for different boundary layer conditions. The different deposition mechanisms are discussed below.

Molecular Diffusion

For solid particles in the size range up to 0.1 μm, particles behave similarly to gas molecules. The gas laws based on kinetic theory control the motion of the particles in much the same way as with gas molecules. Deposition by molecular diffusion decreases with increasing particle size. Gas velocity has no appreciable effect on deposition by molecular diffusion because of the particles being on the molecular size level. As particle size increases, Brownian motion becomes the controlling mechanism for deposition.

Brownian Motion

Particles in the size range of 1 μm diameter or larger behave as discrete pieces of matter. Particles in the range of 0.1 μm to about 1 μm undergo Brownian motion, where collisions with gas molecules establish a "random-walk" path. The flow pattern of these particles depends mainly on the path of the bulk gas stream. Particle displacement by Brownian motion can be described by the equation[16]:

$$\bar{x}^2 = \left(\frac{2k_m T}{c\mu} \right) t$$

(6)
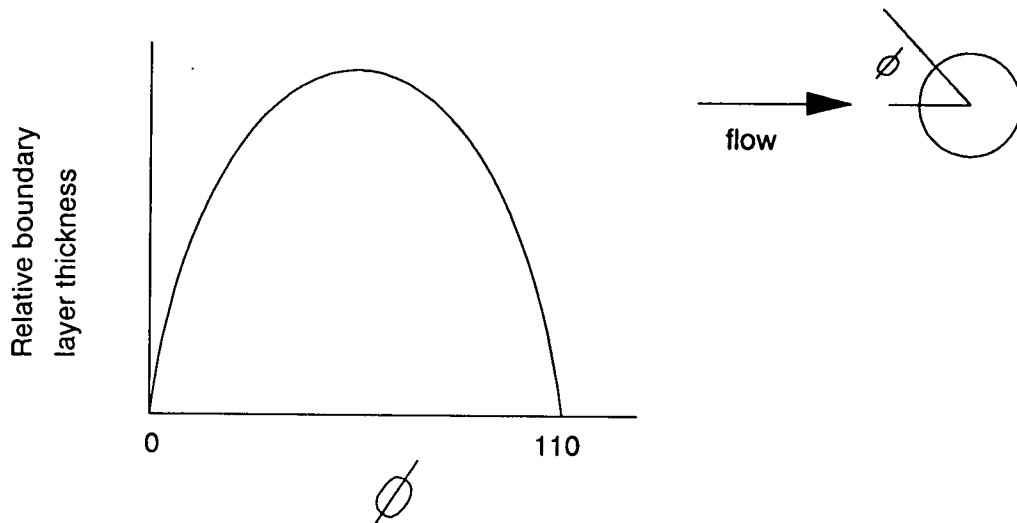
Figure 1. Boundary layer thickness for cylindrical surfaces.

Deposition by Brownian motion increases as the particle size increases, but turbulent diffusion or impaction becomes the dominant mechanism for particles above 1 μm in diameter. The exact point that turbulent diffusion becomes the controlling mechanism over Brownian motion is dependent on the flow system; as the flow rate increases, turbulent diffusion becomes dominant at smaller particle sizes. Brownian motion also becomes dominant over molecular diffusion at smaller particle sizes for greater flow rates. Deposition by Brownian motion can also be influenced by external forces, such as the presence of an electrostatic field or gravity[18].

Turbulent Diffusion

In turbulent diffusion, particles larger than approximately 1 μm enter the turbulent region directly over a solid surface (between the laminar sublayer and the bulk gas stream). These particles then move through the laminar part of the boundary layer to the surface. One method of this transport is explained by Owen; another method is proposed by Davies and by Friedlander and Johnstone.

Owen[19] has found that turbulent bursts sporadically erupt from the laminar layer. He has therefore proposed that particles are convected to the wall in downward sweeps. However, Davies[20] and Friedlander and Johnstone[21] state that in turbulent diffusion particles pick up kinetic energy from gas eddies present in the turbulent boundary layer. These particles are then propelled through the laminar sublayer and onto the surface.

By using particles between 0.8 μm and 2.63 μm, Friedlander and Johnstone[21] studied the deposition of particles by turbulent diffusion. Brownian motion was made negligible by using this particle size range and by using high stream velocities. The experimental apparatus consisted of a circular tube with the gas and particles flowing through the center, and Reynolds numbers varying between 8000 and 50,000. Deposition took place on the sides of the tube, and the authors determined the deposition rates as a function of distance from the inlet; in this way they could follow the development of the turbulent boundary layer. Their results show that deposition occurs only in fully developed turbulent flow. Deposition by turbulent diffusion is a function of both Reynolds number and particle size; deposition increases as both the Reynolds number and particle size increase. Deposition by turbulent diffusion overlaps with deposition by particle impaction; the point at which impaction becomes dominant is a function of system parameters such as flow rate and particle size.

Particle Impaction

Larger particles, on the order of tens of microns in diameter, receive sufficient kinetic energy from the main gas stream for the particles to follow a different path from the propelling gas stream. Particles receiving this kinetic energy are then

relatively unaffected by minor changes in gas direction. Inertial impaction is influenced by gas velocity and the diameter of the collector.

The efficiency of collection of particles due to impaction has been studied by many authors. Fuchs[18] states that in the case of purely inertial deposition on a cylinder the collection efficiency depends only on the Stokes number:

$$Stk = \frac{2l_i}{D} \tag{7}$$

where the stop distance, l_i, is defined as:

$$l_i = \frac{V_\infty d_p^2 \rho_p}{18\mu} \tag{8}$$

The Stokes number, when related to efficiency of inertial deposition on a cylinder, yields results shown in Fig. 2. Theoretical collection efficiency is defined as the fraction of particles in the gas volume swept by the cylinder which will impinge and stick on the cylinder. At large values of Stk, the collection efficiency is close to 1; at values less than 0.2, the efficiency approaches zero. For recovery boiler fume (flue gas velocity=20 ft/sec, d=0.5 μm, ρ_p=2*10^6 g/m^3), Stk=10^{-4}; efficiency for inertial deposition of fume is very close to 0. Efficiency will increase as velocity, particle size, or particle density increases.

Thermophoresis

The movement of aerosol particles due to non-uniform heating of these particles is caused by radiometric forces. Radiometric forces may be caused either by illumination of particles from one side (photophoresis) or by a temperature gradient (thermophoresis)[18]. Photophoresis is due to the gas molecules rebounding from the hotter, illuminated side of the particle with greater velocities than from
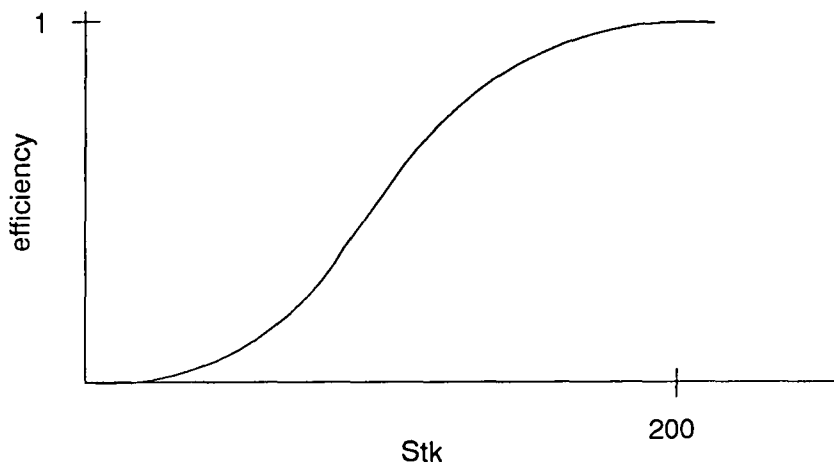
Figure 2. Efficiency for inertial deposition on a cylinder.

the unilluminated side. Particles therefore move away from illuminated, hotter surfaces.

Thermophoresis is the result of gas molecules impinging on the particle from opposite sides with different mean velocities. The molecular bombardment of the particles is more energetic on the hot side than on the cold side, which causes the particles to migrate toward the cooled regions[20,22,23,24]. This will cause particles to be deposited on surfaces that are colder than the gas phase.

Temperature gradients are present around all tube surfaces in the generating bank and economizer regions, with the tubes being cooler than the bulk flue gas. Therefore, if a radiometric force causes fume deposition in the upper sections of a recovery boiler, deposition would be caused by thermophoresis and not by photophoresis.

Wood[22] states that particles which reach the edge of a thermal boundary layer by other mechanisms, such as Brownian diffusion or turbulent diffusion, are subjected to thermophoretic effects because of the large temperature gradient

existing in the boundary layer. Wood's work , and work by others[25,26,27,28], has shown that deposition by thermophoresis is most important for particles between 0.1 μm and 10 μm. In this size range, thermophoresis is dominant over Brownian motion and the particle size is too small for impaction to be a major mechanism.

The total mass flux for a molecular species is given by the equation[29,30,31]:

$$j'' = D_V \left(\nabla \omega_i + \alpha_T \nabla \ln T \right) \tag{9}$$

where the first term is due to Brownian diffusion through a concentration gradient and the second term is due to thermophoresis. This equation applies to particle sizes ranging from vapor molecules up to the size threshold for inertial effects[29,32,33]. For mass flux of fume particles at the cooled tube surface, this equation can be rewritten as:

$$j''_w = \rho_w D_w \left[\left(\frac{\delta \omega}{\delta y} \right)_w + \alpha_{T,w} \omega_w \left(\frac{\delta \ln T}{\delta y} \right)_w \right] \tag{10}$$

Gokoglu and Rosner[29] attempted to solve this equation mathematically by asymptotic analysis, which uses a boundary condition of ω_w=0. This boundary condition, however, would cause elimination of the thermophoretic flux term (the second term in brackets). Therefore, they instead visualized the mass transfer boundary layer to consist of two regions: an exterior region where the mass transport mechanisms are convection and thermophoresis, and an interior region (Brownian diffusion sublayer) where Brownian diffusion becomes important. The Brownian diffusion sublayer thickness is very small and the mass flux to the wall was calculated to be approximately the same as the mass flux through the Brownian diffusion sublayer. Equation 10 can therefore be written as the mass flux through

the Brownian diffusion boundary layer (subscript m) instead of as the mass flux at the wall (subscript w). Equation 11 can now be mathematically solved:

$$j_w'' = \rho_m D_m \left[\left(\frac{\delta \omega}{\delta y} \right)_m + \alpha_{T,m} \omega_m \left(\frac{\delta \ln T}{\delta y} \right)_m \right] \tag{11}$$

$$j_w'' = \rho_m D_m \alpha_{T,m} \omega_m \left(\frac{\delta \ln T}{\delta y} \right)_m \tag{12}$$

$$j_w'' = -\rho_m v_{T,m} \omega_m \tag{13}$$

where the thermophoretic velocity, v_T, is defined as:

$$v_T = -D_v \alpha_T \left(\frac{\delta \ln T}{\delta y} \right) \tag{14}$$

Many authors have published equations, either empirical or theoretical, for thermal velocity. Table 1 lists these authors and their equations. Most authors[28,,35,36,37,38] simply state that:

$$v_T = \frac{K}{T} \left\{ \frac{\delta T}{\delta y} \right\} \tag{15}$$

where K is a function of particle size, particle thermal conductivity, pressure and molecular mean free path[28,35,36,37,38]. Homsy et. al.[36] theoretically calculated that the particle flux to the wall is independent of the nature of the flow; the particle flux depends only upon the physical properties of the gas and particles, and the temperatures of the gas and collector surface.

Both Gokoglu and Rosner[29] and Smith[26] have derived expressions, not containing the temperature gradient form, for thermophoresic velocity. These lead to the following two expressions for particle flux:

Table 1. Thermophoretic Velocity Equations.

Authors	$\underline{v}_T$
Rosenblatt and LaMer[38], 1946	$-\dfrac{K}{T}\dfrac{dT}{dy}$
Smith[26], 1952	$-\dfrac{D\rho_o\lambda_o}{24}\left(\dfrac{d_p}{D}\right)\left(\dfrac{hD}{k}\right)\left(T_e - T_w\right)$
Derjaguin et. al.[37], 1976	$-K\dfrac{\upsilon}{T}\,grad\,T$
Goren[35], 1977	$-K\dfrac{\upsilon}{T}\,grad\,T$
Walker et. al[28], 1979	$-K\dfrac{\upsilon}{T}\,grad\,T$
Vermes[34], 1979	$-K\dfrac{1}{T^{1/2}}\dfrac{dT}{dy}$
Homsy et. al.[36], 1981	$-K\dfrac{\upsilon}{T}\,grad\,T$
Gokoglu and Rosner[29], 1986	$-\alpha_T D_v\left(\dfrac{\delta\ln T}{\delta y}\right)$

$$ \text{G\&R:} \qquad j_w'' = \rho_m V \left(\alpha_T \frac{Pr}{Sc} \right) St_h \left(\frac{T_e - T_w}{T_w} \right) \omega_m \qquad (16) $$

$$ \text{Smith:} \qquad j_w'' = \rho_m \omega_m \left(\frac{D \rho_o \lambda_o}{24} \right) \left(\frac{d_p}{D} \right) \left(\frac{Nu}{\mu} \right) (T_e - T_w) \qquad (17) $$

It is seen that many parameters affect the deposition rate. Some of these factors and their effects will now be discussed.

Particle Concentration (ω)

Both equations agree that the deposition rate is proportional to particle concentration in the gas. The deposition rate will double when the particle concentration is doubled. Obviously, no deposition will occur when the concentration of particles in the gas mixture equals zero.

Particle Diameter (d_p)

Smith's equation predicts that the deposition rate is proportional to particle diameter for all particle sizes. Gokoglu and Rosner's equation also predicts that the deposition rate will increase with increasing diameter; however, this fact is hidden in the Prandtl, Schmidt, and Stanton numbers. Gokoglu and Rosner show that the net result is, for particle sizes between 0.1 μm and 1 μm, the rate of deposition is proportional to particle diameter.

Gas Flow Rate (V)

Smith's equation shows no effect of gas flow on the deposition rate; Gokoglu and Rosner's equation shows a linear relationship ($0 < Re < 10,000$, based on tube diameter). Gokoglu and Rosner's equation, however, is a function of the Stanton number. The Stanton number is inversely proportional to flow rate. The result is

that the gas flow rate should have no significant effect on the rate of deposition by thermophoresis.

Temperature (T)

Gokoglu and Rosner's equation shows a deposition rate proportional to $(T_e-T_w)/T_w$. This is consistent with the definition of v_T, which most authors define to be proportional to $\delta \ln T/\delta y$. Smith's equation, however, predicts a deposition rate proportional to the temperature difference.

Thermal Diffusion Factor (α_T)

The thermal diffusion factor of a particle is a property that will result in different compounds depositing at different rates. It is a dimensionless number and is a function of a particle's molecular properties such as M (molecular weight), σ (Lennard-Jones molecular size parameter), ϵ (Lennard-Jones molecular interaction energy parameter), and local temperature[39]. The magnitude of this number for most fume compounds range from 0.01 to 1. Gokoglu and Rosner's equation shows that the deposition rate is linear with respect to α_T. Smith's equation shows no dependence; it is unknown how Smith deals with differences between compounds.

Vapor Diffusion/Crystallization

When vapor species are present in the gas phase, these constituents are transported across the thermal boundary layer to the tube surface. The mass transfer of volatilized species to a cooled target is due to the difference in partial pressures of the vapor in the bulk gas and that at the deposit surface. If the vapor pressure of the vapor species in the boundary layer gas equals or is greater than the equilibrium vapor pressure at the surface temperature, condensation occurs[32].

Sodium sulfate is one such compound that can deposit by crystallization. Brown[15], Kohl et. al[32], Rosner and Liang[40], Raask[41], and Bishop[42] studied this

deposition and their results indicate the existence of a "dew point" - the surface temperature above which the deposition rate decreases.

Similar results were obtained with other vapor species. Kohl et. al.[32], Rosner and Liang[40], and Raask[41] studied alkali sulfate vapors other than sodium sulfate (such as $CaSO_4$ and K_2SO_4). Bishop et. al.[42,43] studied the deposition of NaCl, and Seshadri and Rosner[44] studied B_2O_3 deposition. All these authors' results show the existence of a dew point, dictated by thermodynamic factors and strongly influenced by transport and kinetic restrictions. If the gas phase temperature is below the dew point, liquid droplets or solid particles will form in the gas. Particles will then be transported to the cooled tube surface by thermal forces and not by vapor diffusion.

Authors disagree on the effects of surface temperature on deposition rate when the temperature is below the dew point. Kohl et. al.[32] and Seshadri and Rosner[44] show that the deposition rate increases linearly with decreasing collector temperature, as shown in Fig. 3. Brown[15], Rosner and Liang[40], Raask[41], and Bishop et. al.[42,43,45] show that the rate of deposition is constant for most temperatures below the dew point, which is depicted in Fig. 4. The important conclusion from all these studies, however, is the realization that a dew point temperature exists. If no deposition occurs above a certain temperature but does occur below this temperature, then vapor diffusion/crystallization is a possible and probable mechanism.

AEROSOL PARTICLE SHAPE AND MORPHOLOGY

It has been found that the shape of deposited particles differs with the particle formation method. Brown[15], Kohl et. al.[32], and Bishop et. al.[42,43,45] have shown in their studies that deposition by vapor diffusion results in crystalline deposits. This
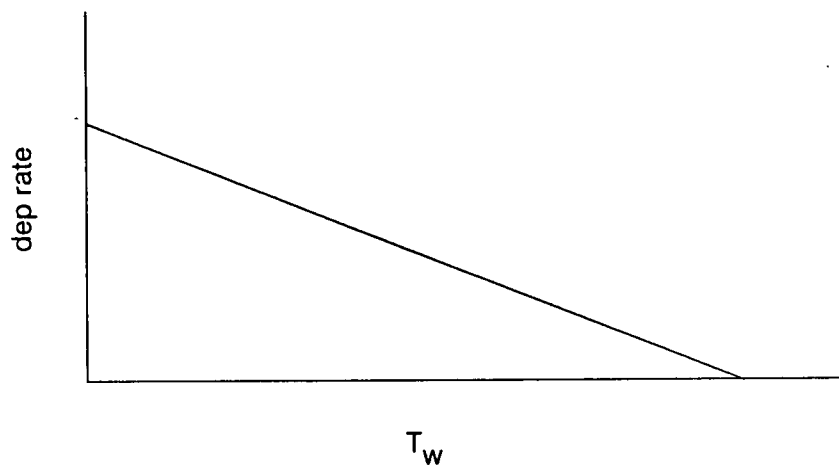
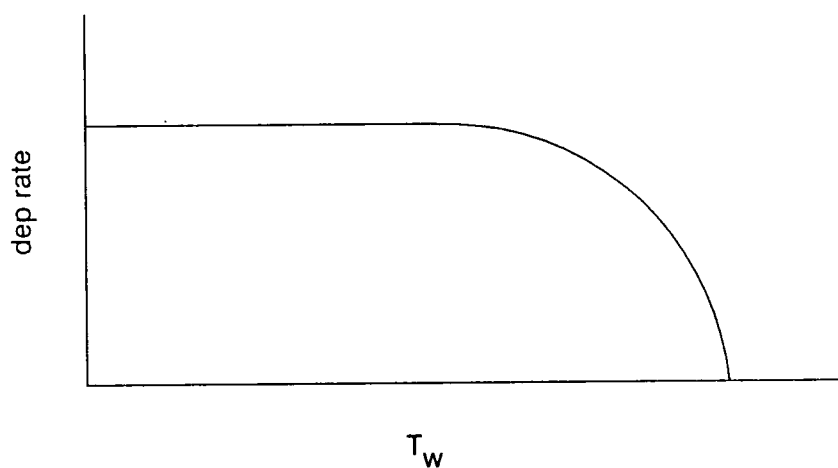Figure 3. Deposition due to vapor diffusion/crystallization, #1.

Figure 4. Deposition due to vapor diffusion/crystallization, #2.

was determined by electron microscopy. Depending on the surface temperature, these crystals were dendritic crystals or elongate square-ended crystals.

Ulrich et. al.[46,47,48,49] and Medalia and Heckman[50] have studied the growth of submicron particles in the gas phase. Their results show that particles, already solid in the gas phase, formed deposits that consisted of aggregates of spherical particles. Particle shape was determined by electron microscopy.

These results show that the structure of the deposited particles is an indication of how the particles were formed.
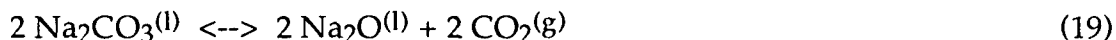
POSSIBLE FUME DEPOSITION MECHANISMS

Sodium Carbonate Deposition

Previous studies[2,12] indicate that solid sodium carbonate fume particles are formed in the gas phase over the smelt bed by the stoichiometric reaction:

$$O_2 + 2\,CO_2 + 4\,Na \longleftrightarrow 2\,Na_2CO_3 \tag{18}$$
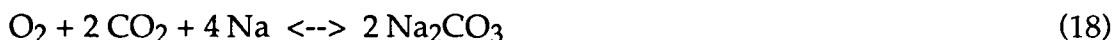
Weaver et. al.[51] has stated that Na_2CO_3 is unstable as a vapor and exists only as a solid and liquid; Motzfeldt[52] states that there should be no chance for significant dissociation at any temperature below 800°C. Recovery boiler smelt is mainly Na_2CO_3, which is another indication that very little sodium carbonate decomposes; otherwise, the smelt would contain smaller amounts of Na_2CO_3. If dissociation did occur, it would be according to the reactions[52,53]:

$$2\,Na_2CO_3^{(l)} \longleftrightarrow 2\,Na_2O^{(l)} + 2\,CO_2^{(g)} \tag{19}$$

$$2Na_2O^{(l)} \longleftrightarrow 4\,Na^{(g)} + O_2^{(g)} \tag{20}$$

The incoming gas temperature to the boiler bank is below 800°C, and the melting point of sodium carbonate is 851°C. At 851°C, the partial pressure of CO_2 due to Na_2CO_3 decomposition is 10^{-6} atm, and the partial pressure of Na_2O is 10^{-3} atm. This indicates that if O_2, CO_2, and Na were all present in the gas phase, Na_2CO_3 would be present as solid particles as the flue gas entered the boiler banks and economizers. This makes vapor diffusion/crystallization an unlikely mechanism for Na_2CO_3 fume deposition.

As mentioned earlier, Na_2CO_3 fume particles have been found to be approximately 0.5 μm in diameter. Deposition by molecular diffusion can therefore be eliminated as a possible mechanism, because fume particles are too large.

It was also mentioned earlier that the Reynolds number in the boiler bank is between 3000 and 5000, which is considered to be in the transition region between laminar and turbulent flow. Friedlander and Johnstone[21] reported that deposition by turbulent diffusion only occurred in fully developed turbulent flow. Vermes' calculations[34] for deposits on cooled turbine blades, at Reynolds numbers between 15,000 and 20,000 (based on blade length), show that thermophoresis is much more significant in causing deposition than turbulent diffusion. If this is true for these high Reynolds numbers, then thermophoresis must be dominant over turbulent diffusion at lower Reynolds numbers; deposition by turbulent diffusion decreases as the Reynolds number decreases while deposition by thermophoresis remains relatively unaffected. Turbulent diffusion, therefore, can also be eliminated as a possible mechanism for sodium carbonate deposition.

Deposition by inertial impaction has been found to be important only for particles greater than 10 μm in diameter[34,39,54,55]; the exact particle size that impaction becomes dominant is dependent on gas velocity. This mechanism will not contribute to deposition of Na_2CO_3 fume particles in the recovery boiler unless Na_2CO_3 fume particles agglomerate to form clusters 10 μm in diameter or larger.

Thermophoresis has been shown to be a large contributer to deposition in the particular size range of fume particles. Brownian movement may account for deposition of some fume particles, but deposition by this mechanism compared to thermophoresis is small[56]. Gokuglu and Rosner[29] show that thermophoresis causes a marked increase in deposition compared to deposition by Brownian motion alone.

This increase can be as much as 1000-fold for 1 μm particles[30,34,54,55]. All these results indicate that deposition by Brownian motion is negligible for deposition on cooled tubes.

The main mechanism for Na_2CO_3 fume deposition, therefore, is likely to be thermophoresis. All other mechanisms will play only a minor role, if any, in deposition.

Sodium Sulfate Deposition

Sodium sulfate's dew point is its melting point (882°C) at 0.15 mm Hg; it rises to 1371°C at 1 mm Hg. If 70% of the fume in the recovery furnace was present as Na_2SO_4 vapor, the vapor pressure would be 0.5 mm Hg and its dew point would be approximately 1200°C. This temperature is hotter than generally found in a recovery boiler, which explains the presence of Na_2SO_4 particles even in the lower sections of the recovery boiler. Therefore, thermophoresis is the likely mechanism for sodium sulfate deposition in all sections of the recovery boiler unless large amounts of agglomeration occur and cause deposition by impaction.

Maule[57] has shown that carbonate conversion to sulfate is dependent on SO_2 concentration, time, and temperature. He also found that sintering of the solid particles, which causes small particles to fuse into larger agglomerates, occurs during the reaction. It has already been stated that particle size affects the deposition rate; if the particles agglomerate, the deposition mechanism as well as the rate might change.

Sodium Chloride Deposition

Sodium chloride fume has a melting point of 801°C and is initially present in the boiler as a vapor. Temperatures in the superheater section are above the NaCl melting point; Sodium chloride should deposit in this area by crystallization or not

at all. Temperatures in the upper sections of a furnace generally are below the melting point of NaCl. NaCl fume should condense from vapor while still in the flue gas; it should then be transported to the cooled surfaces in the boiler bank and economizer sections by the same mechanism as sodium carbonate and sodium sulfate deposition.

RESEARCH APPROACH AND OBJECTIVES

The objective of this research is to develop a model for fume deposition in the boiler banks and economizer. This required the following experiments:

1. Determine if solid particles are present in the gas phase above the smelt surface. This was accomplished by placing a filter directly above the smelt bed. If no particles are present, deposition by thermophoresis or any other solid particle mechanism is impossible.

2. Determine fume generation rate for Na_2CO_3, Na_2SO_4, and NaCl under a range of experimental conditions. The rate of fume deposition can then be related to gas phase fume concentration.

3. Determine what mechanisms are responsible for Na_2CO_3, Na_2SO_4, and NaCl deposition in the upper sections of a recovery boiler and develop a mathemetical model.

Thermophoresis seems the likely mechanism for fume deposition; its controlling parameters are flue gas temperature, tube surface temperature, particle composition and size, particle concentration, and possibly gas flow rate. The experimental study was set up to determine the effect of these variables on deposition rate and therefore to ascertain whether thermophoresis is the actual controlling mechanism.

There are limitations to the experimental system. First, the flue gas flow rate through the experimental system was very limited. Only a Reynolds number of less than 3 (based on cooled tube diameter) could be obtained because of the method of fume generation that was chosen. Gas was bubbled through the smelt to generate fume, and this gas flow was limited because higher flow rates through the melt caused excessive bubbling and splashing of the smelt. The apparatus could not be necked down to a small enough diameter to create turbulent flow; an apparatus diameter of 0.01 inches would have been required. This method of fume generation was chosen, however, because of the excellent control over fume composition and fume purity at these low gas flow rates. Flow differences between the experimental system and an actual recovery boiler may result in differences between calculated and actual deposition rates. Gas velocity was still studied as a variable, but only within the range that the apparatus could handle.

Second, the experimental particle size could be measured but not varied. Particles in the recovery boiler may be agglomerating which will once again cause differences between experimental results and recovery boiler data.

Particle composition was varied by studying Na_2CO_3, Na_2SO_4, NaCl, and simultaneous Na_2SO_4/NaCl fume deposition. Flue gas temperature and tube surface temperature dependence was determined for all four types of fume deposition.

Fume concentration dependence was determined for Na_2CO_3 and NaCl fume. Both deposition rates were found to have the same concentration dependency; Na_2SO_4 and Na_2SO_4/NaCl fume deposition was assumed to follow this dependency as well.

The dependence of fume deposition on gas flow rate was also determined for only Na_2CO_3 and $NaCl$ fume. Once again, it was assumed that Na_2SO_4 and $Na_2SO_4/NaCl$ fume deposition would have the same dependency.

EXPERIMENTAL METHODS

EXPERIMENTAL SYSTEM

The experimental system used to generate fume particles is shown in Fig. 5. Ceramic alumina crucibles (4 $5/16$" i.d., 4 $1/2$" o.d., 15" height) were used to contain the molten smelt. These crucibles could withstand exposure to molten salts over the experimental temperature range and were not reactive with the smelt. The crucible was contained in a stainless steel retort (5 $3/8$" i.d., 5 $1/2$" o.d., 27" height) which was then placed inside a tubular furnace. Exact specifications of this furnace and retort are listed in Appendix II. A small clearance was present between the crucible and retort and between the retort and furnace, which allowed nitrogen to be purged through these areas. Figure 6 is a schematic of the crucible-retort-furnace design.

All gases were obtained from pressurized gas cylinders, and the volumetric flow rates of these gases into the reactor were determined by dry-gas meters. Two mercury manometers, one connected to the N_2 line and one to the CO_2 line, were used as safety valves. The N_2 and air streams were mixed before reaching the reactor. This gas mixture then flowed into the crucible by means of a ceramic purge tube (18" long, $3/16$" i.d., $1/4$" o.d.) which extended into the molten salts and caused mixing of the reactants. The CO_2 could be introduced into the reactor in two ways: either into the N_2/air stream so the CO_2 would flow into the crucible below the melt, or above the melt so the CO_2 would be mixed with the flue gas in the reactor.

A K-type thermocouple ($1/8$" diameter), good for a temperature range of up to 1400°C, monitored the molten salt temperature. The thermocouple was contained in a ceramic tube (18" long, $1/4$" i.d., $3/4$" o.d., closed at one end) which extended into
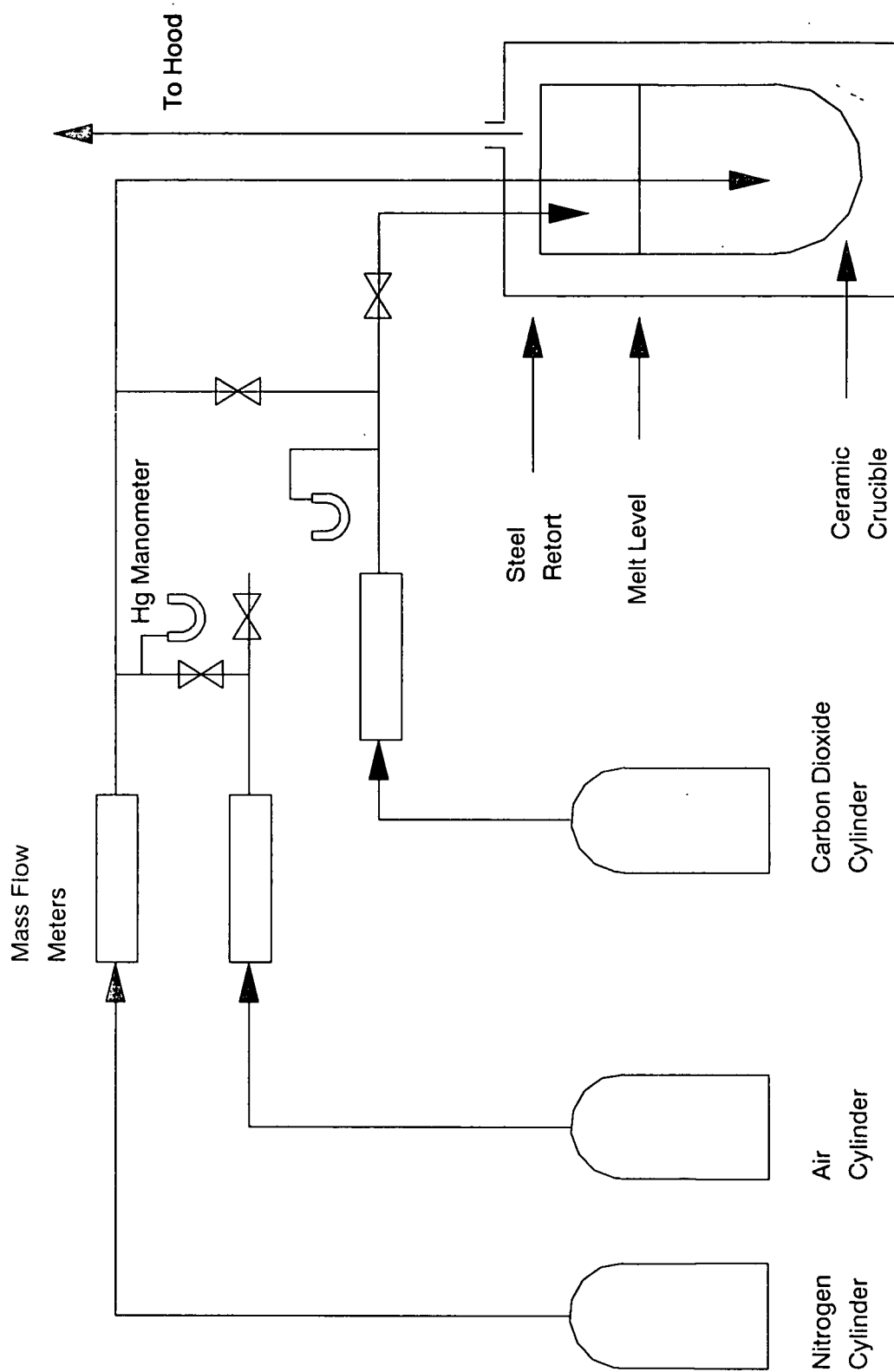
Figure 5. Fume generation system.

Thermocouple

Nitrogen and Air Inlet

Carbon Dioxide Inlet

Flue Gas Outlet

Electric Tubular Furnace

Melt Level

SS Retort

Ceramic Crucible

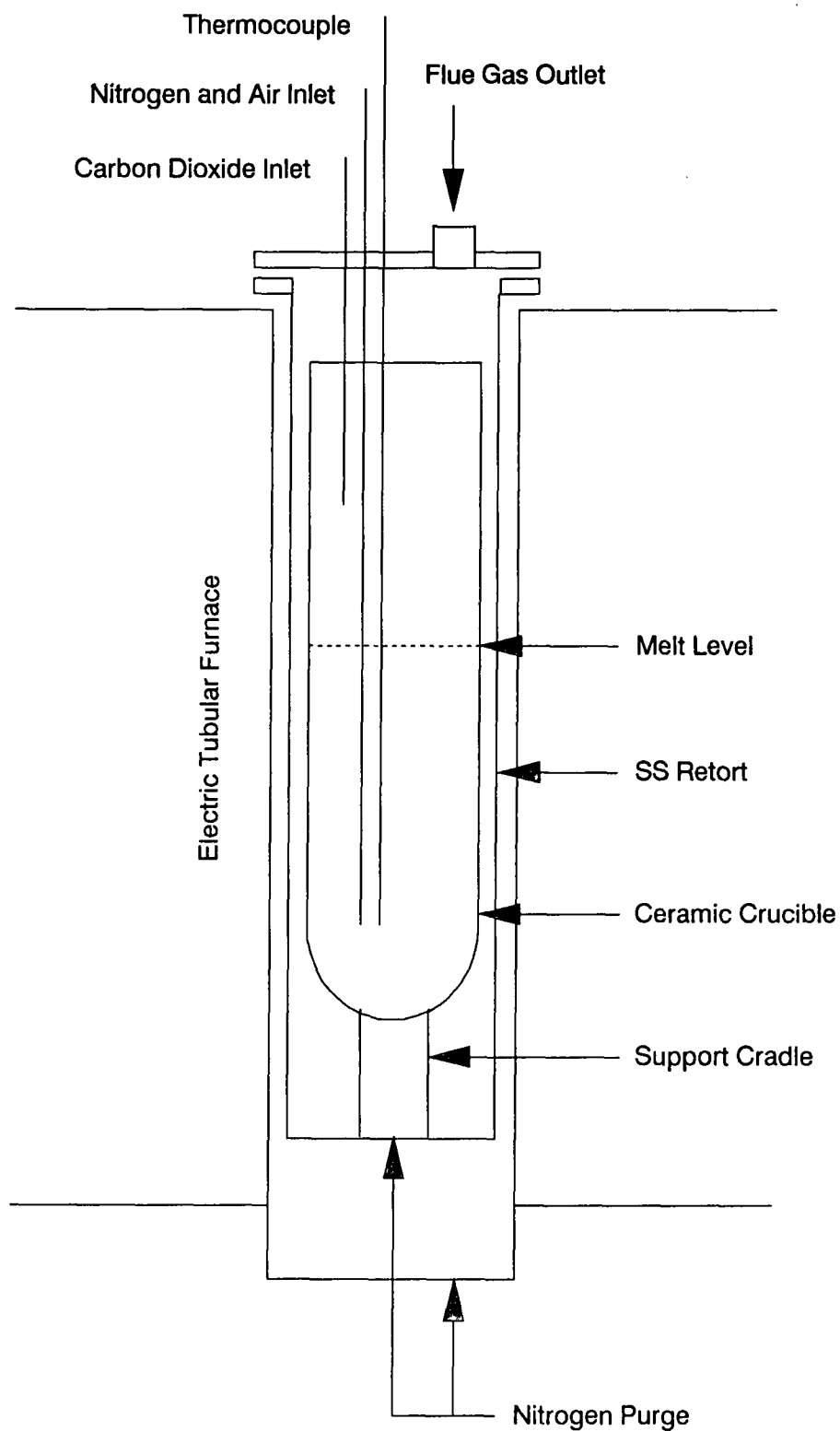Support Cradle

Nitrogen Purge

Figure 6. Crucible-retort-furnace schematic.

the smelt. Generated fume and flue gas was vented to the hood after leaving the reactor.

CHEMICALS

The following chemicals were used:

1. Na_2CO_3, anhydrous, granular, reagent grade.

2. Na_2S, reagent grade.

Sodium sulfide was purchased as $Na_2S \cdot 9H_2O$; the water must be removed before placing the Na_2S in the furnace. Water was removed by drying the sodium sulfide in a vacuum oven with a nitrogen purge. The oven was brought to a drying temperature of 190°C within a span of approximately six hours and was kept at 190°C for 24 hours. The long heat-up time prevented excess splashing of the water in the sulfide. The resulting chemical was dry Na_2S, which was then coarsely ground with a mortar and pestel in a glove box.

In this thesis, all flow rates listed as L/min are standard liters per minute.

EXPERIMENTAL PROCEDURE

In most runs, 2200 g (20.8 moles) of sodium carbonate were placed in the crucible. The crucible, contained in the electric furnace, was brought to the reaction temperature within a span of ten to twelve hours to decrease the chance of the crucible cracking. During the heat-up period nitrogen was continuously purged through the inlet tube under the Na_2CO_3 surface at a rate of 0.2 L/min, thus preventing inlet tube plugging. A nitrogen purge was also present both inside and outside the retort, preventing excess corrosion of the retort.

After the crucible temperature was stabilized at the reaction temperature, approximately 200 g (2.6 moles) of dry Na_2S were added, through a 2" diameter hole

in the retort cover, to the molten Na_2CO_3. The N_2, air, and CO_2 flow rates were then brought to the levels to be used during the experiments.

Once the system reached steady state with these new flow rates, experimental data were taken. The run was continued until all the Na_2S had reacted with the incoming air; another 200 g Na_2S was then added and the run continued. Na_2S was added to the smelt as many times as necessary so a complete set of data could be obtained. Cameron's work[2] has shown that the level of sulfide and sulfate in the melt has no significant effect on the rate of fume generation. Therefore, the addition of Na_2S during the course of the experiment did not change the fume generation rate.

RADIANT ENERGY EFFECTS

Radiant energy from smelt beds or smelt pools have been found to affect gas phase thermocouple readings. An unshielded thermocouple would be expected to measure a higher temperature than a shielded thermocouple. This is especially true at higher temperatures and in close proximity to the smelt bed. Therefore, the effect of radiant energy on the experimental gas phase thermocouple must be determined.

In order to determine the radiant energy effects on a gas phase thermocouple, an aspirated thermocouple was constructed. The thermocouple, shown in Fig. 7, was surrounded by a stainless steel tube ($3/16$" i.d., $1/4$" o.d.) with small holes drilled into the bottom of the tube. Suction was placed on the top end of the tube, so the flue gas was drawn through the bottom of the tube and forced into contact with the thermocouple end. The tube shielded the thermocouple from radiation effects. This shielded thermocouple was placed directly into the furnace at different levels above the melt.
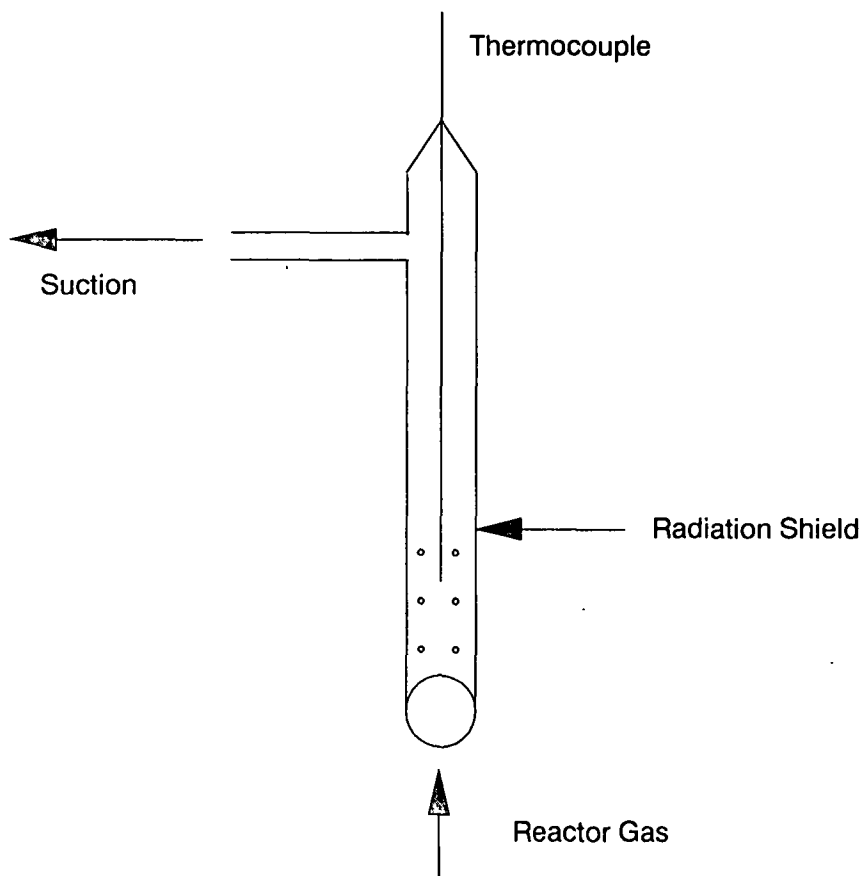
Figure 7. Aspirated thermocouple design.

The temperatures obtained from the aspirated thermocouple were compared to the values obtained from an unshielded thermocouple placed in the reactor in the same manner as the aspirated thermocouple. The difference in the measured temperatures from the two thermocouples would be due to this radiation. The thermocouples were documented to be accurate to 0.75%, or 6°C at a temperature of 800°C.

No fume was generated for this experiment, but N_2 was continually purged into the smelt at a flow rate of 3 L/min. Nitrogen flow was used so there would be

an upward flow of gases past the thermocouple. The rate of suction was 8 L/min which produced a Reynolds number, past the thermocouple end, of 450,000. This insured that the gas phase temperature was actually being measured.

Radiant energy was found to have a minimal effect on the gas phase thermocouple reading, as shown in Fig. 8. If thermocouple accuracy is taken into account, the difference between the two thermocouple readings can be considered negligible below a temperature of 800°C. At 600°C, the thermocouple accuracy is 4.5°C; Fig. 8 shows a measured temperature difference, between the two thermocouples, of less than 4.5°C. Gas temperatures above 600°C were never encountered during fume deposition for this thesis; therefore, a shielded thermocouple was not required.

FUME GENERATION

The objective of these experiments was to model the fume generation rate in terms of gas flow rates, melt composition, and melt temperature. This model could then be used to determine deposition rates as a function of fume concentration. The experimental furnace used to generate fume is shown in Fig. 9. The fume was caught on a 3" diameter glass microfiber filter, which could easily be disconnected from the system. This filtering system, shown in Figure 10, consisted of poly-flo tubing leading from the reactor to the filter, and a "filter holder" which held the filter in place. The fume generation rate was calculated by weighing the fume that was collected in a given time span.

The tube leading from the reactor to the filter tended to plug with fume. For this reason, a 2" hole in the retort cover was used as a "relief hole" with a metal weight placed over the hole. When the outlet tube become plugged, the metal
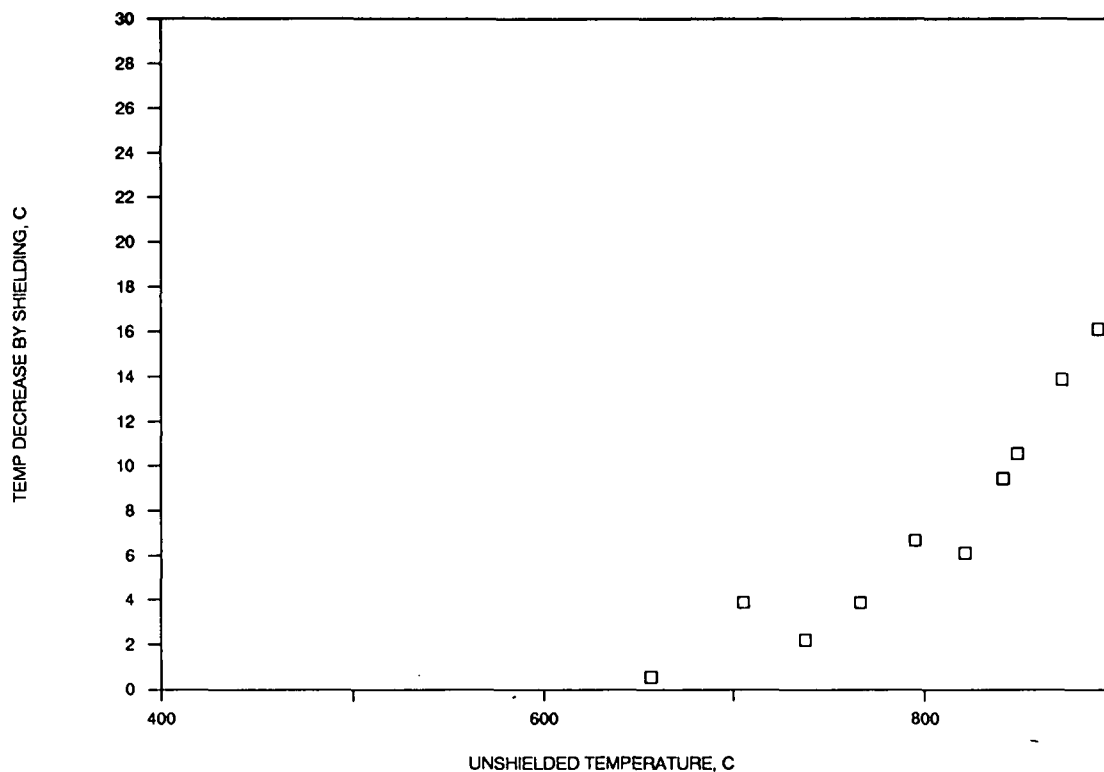
Figure 8. Effect of radiation shielding.

weight shifted and allowed gases to escape through the relief hole. The outlet tube was then cleaned and the experiment continued.

The fume that plugged the outlet tube built up over the course of about an hour. The amount of fume needed to plug the tube was on the order of the amount collected on the filter for one data point, with the potential for obtaining 50 data points per hour. The fume caught in the line can therefore be considered negligible.

Using this approach, fume generation rates were measured for Na_2CO_3, Na_2SO_4, and NaCl generation under different experimental conditions and for simultaneous Na_2SO_4/NaCl generation under one specific set of conditions.
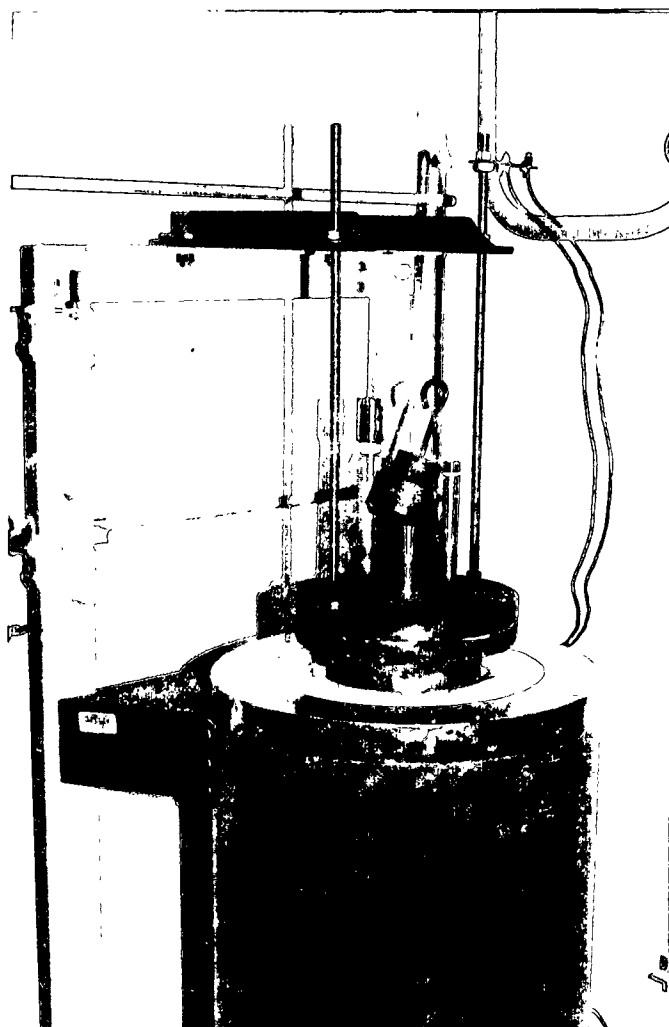
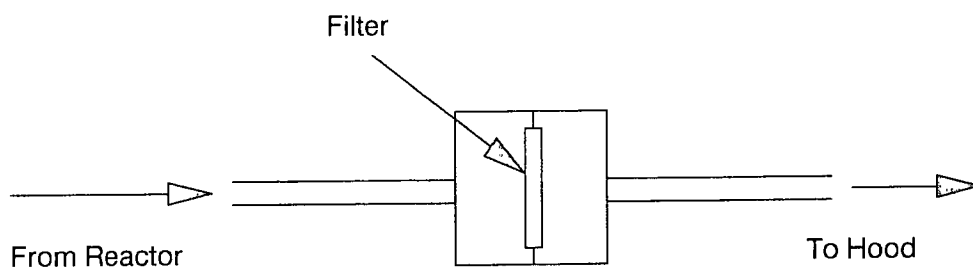Figure 9. Furnace for fume generation.

Figure 10. Schematic of fume filter.

It was assumed that very little fume collects on the sides of the reactor compared to the amount of fume that is collected on the filter. This amount was not measured but it was noticed that, once the apparatus was dissassembled after a complete experimental run (about three hours of fume generation), very little fume had deposited on the reactor sides. The amount of fume collected is therefore considered equal to the amount of fume generated.

Na_2CO_3 Generation

For Na_2CO_3 generation, the following range of variables was used:

1. 2.02-6.18 L/min N_2 under melt surface.

2. 0.19-0.87 L/min O_2 under melt surface.

3. 900-1030°C melt temperature

The following equation was developed:

$$\text{Fume gen. (g/min)} = 20.19 * O_2^{0.218} * N_2^{0.915} * e^{-15690/RT} \tag{21}$$

The flow rates are in liters/minute and the temperature is in °K.

The rate of fume generation was also found to decrease with increasing CO_2 concentration. A comparison of this equation to that obtained by Cameron[2] at The Institute of Paper Chemistry, and the error limits associated with these equations will be discussed later.

Various analyses were performed on the generated fume. An x-ray diffraction pattern showed that Na_2CO_3 fume molecules were crystalline in nature, not amorphous. A scanning electron micrograph showed that the fume particles were approximately 0.5 μm in diameter, and ranged from 0.25 μm to 1 μm in diameter (see Fig. 11). The particles were smooth and round, which implied that
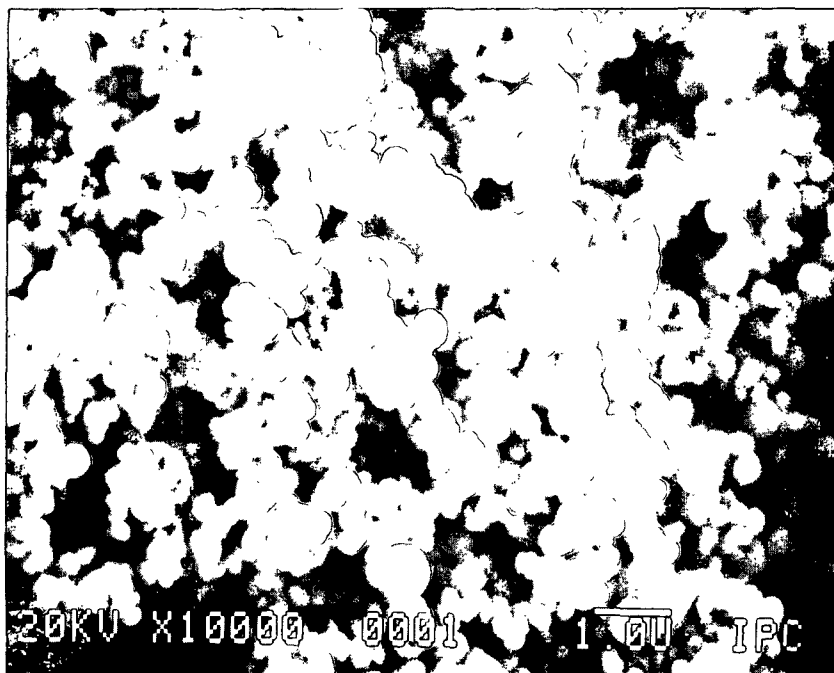
Figure 11. Generated Na2CO3 fume.

individual particles froze from a liquid phase. The particle size, found by image analysis, was 0.30 μm with a variance of 0.0051.

Na2SO4 Generation

For Na2SO4 generation, SO2 was added above the melt surface. The objective was to determine a set of conditions where the majority of sodium carbonate would be converted to sodium sulfate within the first minute. It would therefore be known that the conversion took place in the gas phase and not on the deposition tube. The range of variables studied was:

1. 1.79-5.37 L/min N2 under melt surface.

2. 0.21-0.63 L/min O2 under melt surface.

3. 0.0023-0.0320 L/min SO2 above melt surface.

4. 0.50-7.07 L/min N2 above melt surface.

5. 950°C melt temperature.

The SO_2 and N_2 above the melt surface was from a N_2/SO_2 gas cylinder, 0.45% SO_2. It was found that, in the time it took for the fume particles to reach the filter (approximately 15 seconds), over 70% of the Na_2CO_3 had reacted to form Na_2SO_4 under the following conditions:

1. 1.79 L/min N_2 under melt surface.
2. 0.21 L/min O_2 under melt surface.
3. 0.02 L/min SO_2 above melt surface.
4. 3.98 L/min N_2 above melt surface.
5. 950°C melt temperature.

This set of conditions was used later during the experiments concerning Na_2SO_4 deposition. These conditions also produced the same flow rate and fume concentration as used during Na_2CO_3 deposition.

Electron micrographs of Na_2SO_4 fume, collected from the flue gas, showed particles very similar to Na_2CO_3 fume. The particles were smooth and spherical, and ranged from about 0.25 μm to 1 μm in diameter (see Fig. 12). The particle size was 0.29 μm with a variance of 0.0061.

<u>NaCl Generation</u>

For NaCl generation without sodium carbonate or sodium sulfate generation, all Na_2S present in the melt was first converted to Na_2SO_4. NaCl was then added to the melt. Nitrogen was purged through the system and NaCl vaporized into this N_2 stream; the flue gas cooled as it travelled up the apparatus which caused the sodium chloride to condense. Condensed NaCl was then collected on a filter in the same manner that Na_2CO_3 and Na_2SO_4 were collected.
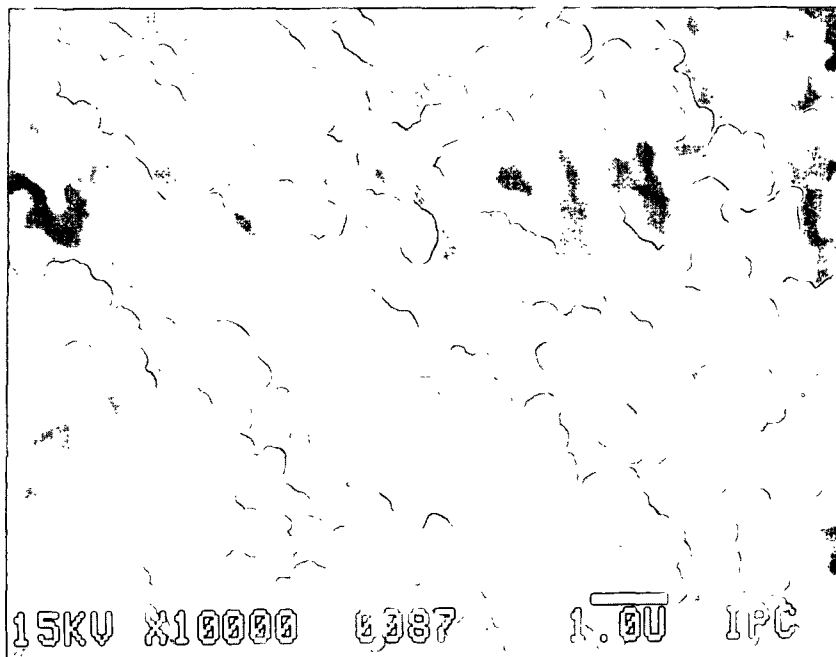
Figure 12. Generated Na_2SO_4 fume.

The range of variables was:

1. 200 & 1000 g (13 & 42 mole %) NaCl in melt.

2. 2.00-8.00 L/min N_2 below melt surface.

3. 0-4.00 L/min N_2 above melt surface.

4. 950°C melt temperature.

The predicted fuming rate, using Raoult's law and assuming that the concentration of NaCl in the gas phase is in equilibrium with the concentration in the melt, was different than the actual fuming rate. If the total N_2 flow is used in the calculation, the predicted fuming rate is approximately 45% higher than actual; if only N_2 flow below the melt is used in the calculation, the predicted rate is approximately 50% lower than observed. This suggests that the gas phase is not in equilibrium with the melt due to nitrogen being added above the melt surface.

Although no electron micrographs were taken of generated NaCl fume, other work at IPC[58] has shown that NaCl fume consists of spherical particles approximately 0.25 µm to 1 µm in diameter. This result is the same as that for Na_2CO_3 and Na_2SO_4 fume generation; Na_2CO_3 and Na_2SO_4 fume particles were spherical and 0.25 µm to 1 µm in diameter.

Na_2SO_4/NaCl Generation

For simultaneous Na_2SO_4 and NaCl generation, the melt consisted of Na_2CO_3, Na_2S, and NaCl. Nitrogen and air were bubbled through the melt to generate both Na_2CO_3 fume and NaCl fume; SO_2 was added above the melt surface to convert Na_2CO_3 to Na_2SO_4. The set of variables was:

1. 1000 g (42 mole %) NaCl in melt.

2. 1.79 L/min N_2 below melt surface.

3. 0.21 L/min O_2 below melt surface.

4. 0.0018 L/min SO_2 above melt surface.

5. 4.00 L/min N_2 above melt surface.

6. 950°C melt temperature.

The large mole % NaCl was used to produce a large enough generation rate for accurate measurement. This amount produced a NaCl generation rate one-third that of the Na_2SO_4 generation rate.

It was determined that Na_2SO_4 fume generation and NaCl fume generation are independent reactions; the fume generation rates were found to be additive within 1% error. The generation rate of sodium sulfate fume (in a system with no sodium chloride fume generation) plus the generation rate of sodium chloride fume (in a system with no sodium sulfate fume generation) was the same as the total generation rate when both Na_2SO_4 fume and NaCl fume were being produced.

An electron micrograph of combined $Na_2SO_4/NaCl$ fume is shown in Fig. 13. These particles looked very similar to Na_2SO_4 fume; particles were smooth and spherical with a size range of 0.25 μm to 1 μm in diameter. Each fume particle was found, by energy dispersive spectrometry, to contain both NaCl and Na_2SO_4. No particle was pure NaCl or pure Na_2SO_4. It is unknown, however, if these two compounds are randomly placed throughout the particle or if one compound formed over the other compound.

FUME COLLECTION DIRECTLY ABOVE MELT

In order for fume to deposit by thermophoresis, solid particles must be present in the gas phase above the smelt bed. These solid particles could be caught by a filter placed directly in the furnace. Solid particles, if any are present in the flue gas at these elevated temperatures, would become entrapped on the filter; the flue gas and any vapor would pass through.

This set of experiments was therefore designed to capture fume particles at the elevated temperatures directly above the melt. Fume was collected by placing the filter in the furnace and drawing a suction through the 1" diameter filtering device shown in Fig. 14. The filtering material, its properties, and the reasons for choosing this material are given in Appendix III.

The filter could only be lowered to approximately three inches above the melt - the smelt from the bed otherwise splashed onto the filter. This splashing occasionally caused the filter to fall out of the filter holder. It was found that the amount of fume collected per volume of suctioned gas was constant, therefore, if the suction flow rate changed, the total amount of collected fume also changed. The suction flow rate could fluctuate as much as 25%; therefore, the flow rate was closely monitored.
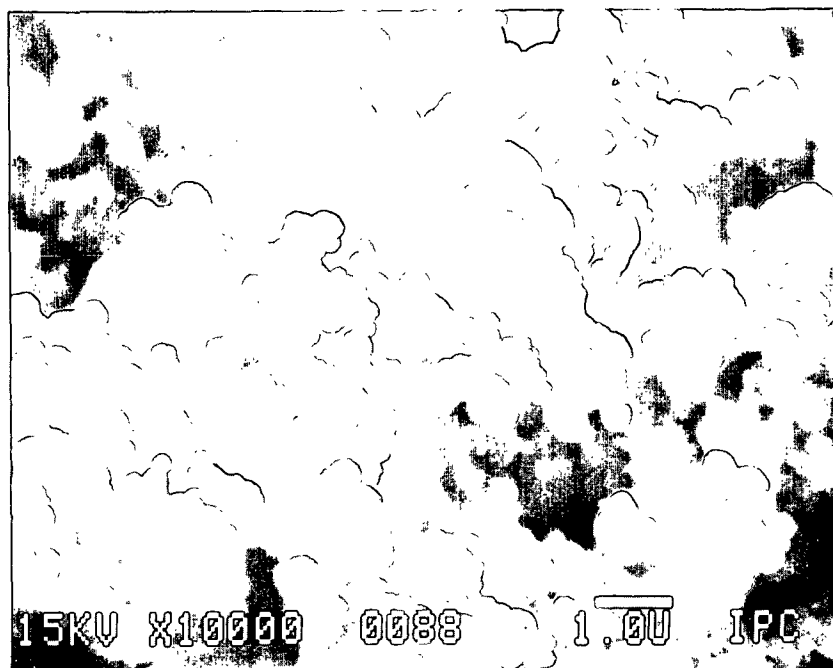
Figure 13. Generated $Na_2SO_4/NaCl$ fume.

Fume was collected at different heights from the smelt bed. All of the data were taken under these conditions:

1. 5.37 L/min N_2 under melt surface.

2. 0.63 L/min O_2 under melt surface.

3. 970°C melt temperature.

4. 8.0 L/min suction.

5. 30 second collection time.

Table 2 lists the results from these experiments. It also lists the amount of fume that should have been collected in each case, calculated by knowing gas flow rates through the filter and fume generation rate. These data show that fume particles were formed within three inches of the smelt bed, and that the amount of fume present has no correlation to the distance from the smelt surface. This
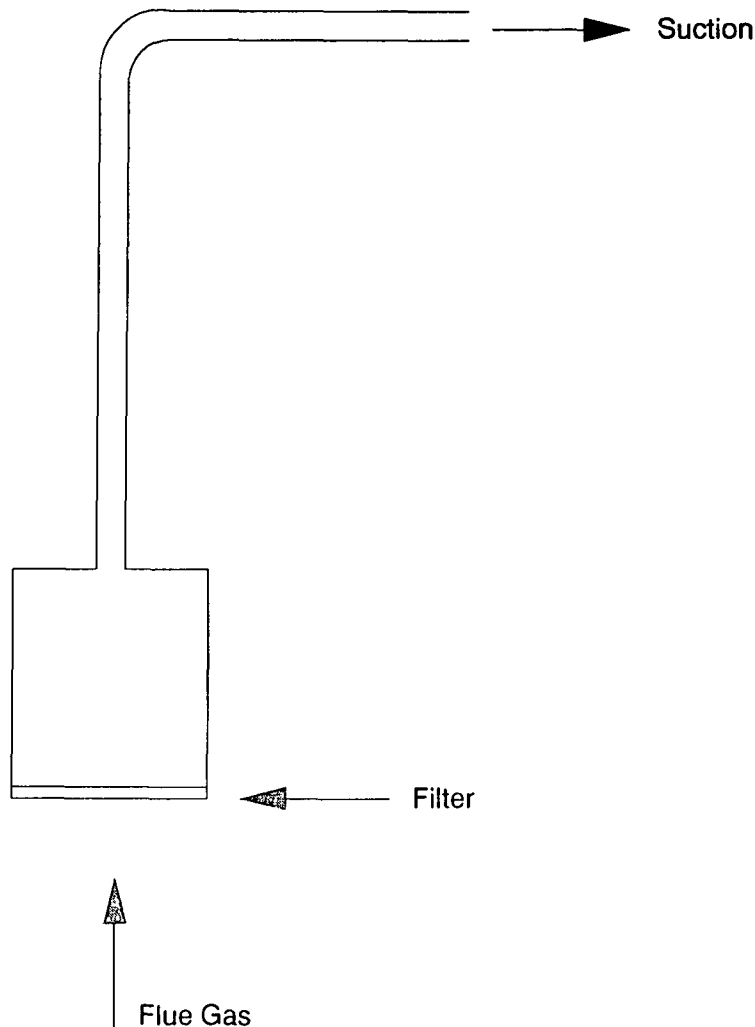
Figure 14. Fume filtering device for directly above smelt surface.

indicates that neither gas temperature nor time in the gas phase has any relation to fume generation. A distance of three inches above the smelt bed corresponded to a gas temperature of approximately 870°C; a time of about four seconds was needed for the gas to travel three inches.

SEM pictures were taken of the fume collected at all heights and all fume generation rates. These pictures showed particles ranging in size from 0.25 μm to over 3 μm, which is a much broader size range than that previously observed.

Table 2. Fume collection from above smelt.

Height above smelt, inches	fume, g/30 sec		
	Predicted	Collected	St. dev.
3	0.0755	0.0757	0.0162
6	0.0755	0.0659	0.0069
9	0.0755	0.0666	0.0083
9	0.0157	0.0153	0.0022
9	0.0171	0.0158	0.0017
9	0.0183	0.0199	0.0016

These new pictures were taken of fume particles captured in the gas stream with gas temperatures of 700°C to 870°C; previous pictures were taken of particles filtered from a much cooler flue gas, outside of the furnace. It will be shown later that these large fume particles must have grown to this size after being captured on the filter - not by small particles colliding with each other in the gas phase.

EXPERIMENTAL SYSTEM FOR FUME DEPOSITION

A schematic of the system used to study fume deposition on a cooled tube is shown in Fig. 15. The lower half of this apparatus was the same as that previously used. The upper half, made of stainless steel and 24" long, clamped onto the lower retort and increased the vertical distance in which the gas travelled before leaving the apparatus. The K-type thermocouple ($1/8$" diameter) extended downward from the top, and the purge tube and melt thermocouple entered the crucible at an angle from the side of the retort. Carbon dioxide or sulfur dioxide entered from the side of the upper half.
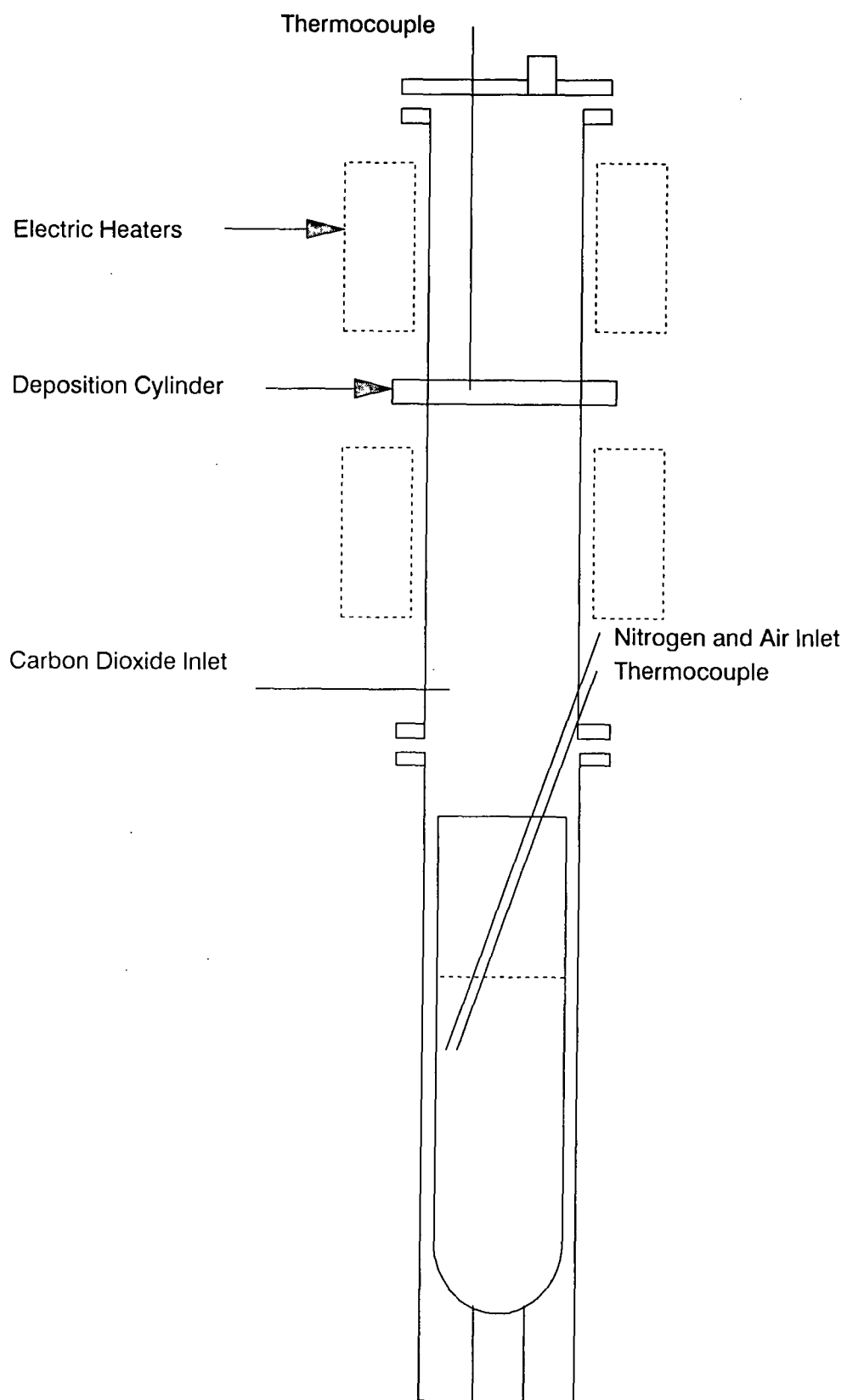
Figure 15. Schematic of fume deposition apparatus.

Electric heaters, one set below the cooled tube and one set above the tube, were added so the gas phase temperature could be varied. This is shown in Fig. 16. Each set of heaters was connected to its own rheostat. These heaters reached temperatures as high as 700°C, which produced a flue gas temperature of 560°C in the area of the cooled tube; the heaters allowed a flue gas temperature range of 280°C to 560°C. Exact specifications for the heaters are listed in Appendix IV.

Fume was collected on the surface of the tube placed in the upper part of the apparatus. The tube was $7/8$" o.d. 304L stainless steel tubing with a wall thickness of 0.035", and was held in place on each side of the apparatus by a flange and set screw (see Fig. 17). This tube was 23 inches above the melt surface; approximately 30 seconds was required for the flue gas to travel from the melt to the tube surface. This corresponds to a Reynolds number of 3 based on cooled tube diameter.

The surface temperature of the tube was determined by inserting a thermocouple through the tube to the surface. A chromel-alumel thermocouple with glass insulation was brought through the inside of the tube and then through small holes in the metal (the two wires were brought through separate holes). The wires were then twisted together and peened in place on the surface. The surface temperature was controlled by air flowing inside the tube. As the coolant flow rate increased, the surface temperature decreased. An increase in the coolant flow from 2 ft^3/min to 8 ft^3/min produced a surface temperature decrease in the range of 30% to 60%; the exact decrease depended on flue gas temperature.

PRELIMINARY RESULTS

A preliminary experiment was performed in order to determine the presence or absence of a temperature difference between the upstream (bottom) side and downstream (top) side of the tube. The average encountered temperature difference
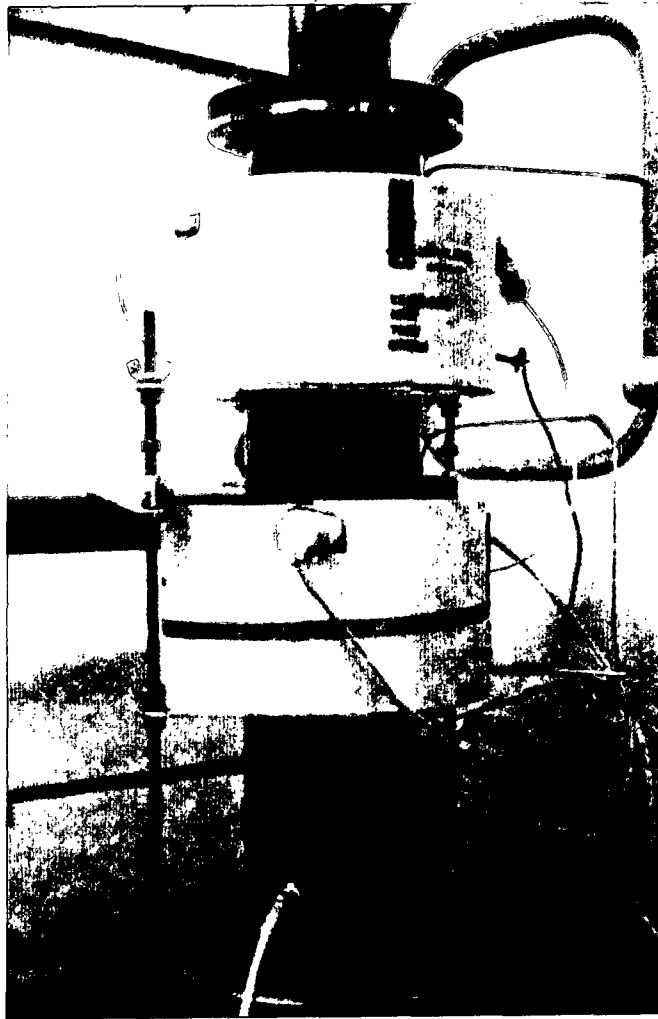
Figure 16. Apparatus for fume deposition.

was 15°C. All surface temperature readings in this thesis, unless specified, are reported as the temperature on the top side of the tube.

Another experiment was performed to determine the extent of a horizontal temperature gradient across the cooled tube. This gradient would be caused by the coolant increasing in temperature as it travels through the tube, or from an entrance length effect. For these experiments, three thermocouples were positioned on the tube: one close to the coolant entrance, one close to the coolant exit, and one in the middle. It was found that, at the most extreme conditions used (high flue gas
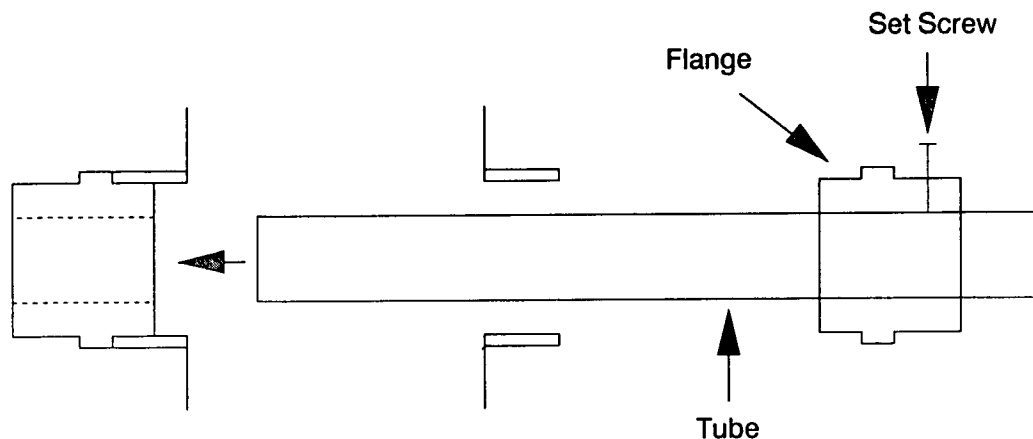
Figure 17. Schematic of cooled deposition tube.

temperature, low coolant flow), the horizontal temperature difference was 94°C. Under all conditions, however, the surface temperature reading of the middle thermocouple was found to be approximately the same (slightly lower) as the reading close to the exit. It was assumed that most of the tube surface was at the temperature close to the middle temperature reading; this reading was therefore used as the average tube surface temperature for all experiments in this thesis. At the most extreme conditions (high flue gas temperature, low coolant flow), if the first $1/4$ of the tube is assumed to rise linearly in temperature and the last $3/4$ is assumed to be a constant temperature, the error in fume weight by assuming a constant temperature is 16%.
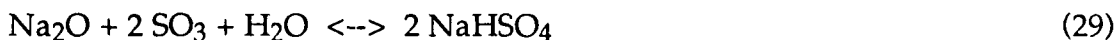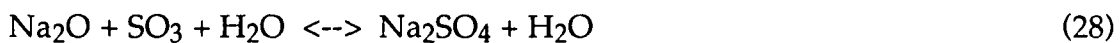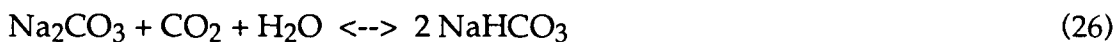
FUME DEPOSITION EXPERIMENTS

The deposition of pure Na_2CO_3 was studied first. CO_2 was added to the gas phase to insure complete conversion of all sodium vapors to sodium carbonate. Extremely small amounts of water were found to have significant effects on the fume composition. When water was present, the fume (which should have been 100% Na_2CO_3) consisted of the following:

1. Na_2CO_3.

2. $Na_4CO_3SO_4$.

3. $Na_6(CO_3)_2SO_4$.

4. $Na_6CO_3(SO_4)_2$.

5. Na_2SO_4.

Generation of Na_2CO_3 fume required a Na_2CO_3/Na_2S melt; the sulfide in these fume compounds therefore came from the smelt bed. The reactions forming these compounds occurred very quickly and were found not to be affected by temperature (gas or surface), CO_2 partial pressure, or time. With H_2O present, this fume mixture was approximately 10% Na_2CO_3, 80% double salts, and 10% Na_2SO_4 under all experimental conditions, which suggests that fume composition in a recovery furnace should be mostly sulfur containing compounds..

Water vapor can react with many compounds in the experimental apparatus. The following stoichiometric reactions are possible:

$$2 SO_2 + O_2 \longleftrightarrow 2 SO_3 \tag{22}$$

$$H_2O + CO \longleftrightarrow H_2 + CO_2 \tag{23}$$

$$H_2 + Na_2S \longleftrightarrow H_2S + 2 Na \tag{24}$$

$$Na_2CO_3 + H_2O \longleftrightarrow 2 NaOH \tag{25}$$

$$Na_2CO_3 + CO_2 + H_2O \longleftrightarrow 2 NaHCO_3 \tag{26}$$

$$Na_2O + H_2O \longleftrightarrow 2 NaOH \tag{27}$$

$$Na_2O + SO_3 + H_2O \longleftrightarrow Na_2SO_4 + H_2O \tag{28}$$

$$Na_2O + 2 SO_3 + H_2O \longleftrightarrow 2 NaHSO_4 \tag{29}$$

$$2 \, Na + 2 \, H_2O \longleftrightarrow H_2 + 2 \, NaOH \qquad (30)$$

$$Na_2S + 4 \, H_2O \longleftrightarrow Na_2SO_4 + 4 \, H_2 \qquad (31)$$

Sodium hydroxide then react with sulfur gases to form Na_2SO_4. The presence of intermediates, such as $NaHSO_4$, in the reaction sequence could also explain the presence of the double salts in the experimental flue gas.

These reactions can be occurring in a recovery boiler in addition to occurring in this experimental apparatus. The reaction of sodium compounds in the gas phase, particularly Na_2CO_3 fume with water vapor, may be one reason that fume consists of mostly sodium sulfate and very little sodium carbonate. The amount of water vapor in a recovery furnace (15% by volume) is 100 times the amount of water needed to convert all Na_2CO_3 fume to other compounds. If all Na_2CO_3 fume in the recovery boiler reacted with H_2O, no sodium carbonate fume would be present. Na_2CO_3, however, is present in a recovery boiler, which shows that not all Na_2CO_3 reacts with water vapor. These results show that Na_2SO_4 fume could also be forming by direct reactions with smelt in addition to being formed by conversion of Na_2CO_3 fume.

These double salts and Na_2SO_4 in the experimental flue gas could be eliminated by eliminating the water in the system. This was accomplished by adding a tube filled with Drierite to the gas lines coming from the air cylinder and the CO_2 cylinder.

The effects of the following variables on Na_2CO_3 deposition were then determined (see Appendix V for tabulations of experimental data):

1. Gas flow rate: varied by adding N_2 above the melt and increasing O_2 partial pressure to keep flue gas fume concentration the same.

2. Fume concentration: changed by varying the CO_2 concentration in the
   gas phase while keeping the total flow rate constant.

3. Tube surface temperature: varied by increasing or decreasing the
   amount of air coolant flowing through the cylinder.

4. Flue gas temperature: changed by varying the rheostat settings on the
   electric heaters.

Na_2SO_4 deposition was studied next. The effects of the following variables
were determined (see Appendix VI for experimental data tables):

1. Tube surface temperature.

2. Flue gas temperature.

Third, NaCl deposition was studied. These experimental parameters were
varied (see Appendix VII for data):

1. Fume concentration: varied by adding different amounts of NaCl to
   the melt.

2. Tube surface temperature.

3. Flue gas temperature.

Finally, the deposition of Na_2SO_4 and NaCl was combined. The effects of tube
surface temperature and flue gas temperature on the rate and mechanism of this
simultaneous deposition were studied. This group of data is tabulated in Appendix
VIII.

Electron micrographs of all fume deposits were taken, which determined
particle size and shape (spherical or needle-like). Image analysis was then used to
determine particle size distribution. The amount of fume on the tube was
determined gravimetrically by fume being scraped off the tube and into a weighing
dish; the fume was then weighed to the nearest 0.0001 g on an analytical balance.

Some fume samples were washed off the cooled tube with water instead of being scraped off the tube with the water being evaporated before weighing the fume. This method produced the same results as the "scraping" method, but was more time-consuming. It also changed the original size and shape of the deposited fume particles. Therefore, the scraping method was used.

THEORETICAL ANALYSIS

FUME GENERATION RATE

Fume generation can be modelled either theoretically or empirically. In theory, the fume generation rate should be proportional to $\ln(K_2*O_2$ flow$)$[59]. It should also be proportional to the N_2 flow. It was assumed that there is an Arrhenius temperature dependence on the rate of fume generation. This gives rise to the following rate equation[14]:

$$\text{Fume generation rate} = K_1 * \ln(K_2*O_2) * N_2 * e^{-\Delta E/RT} \tag{32}$$

Another possible way of calculating fume generation rate is by using an empirical model. The following empirical equation has been found to fit fume generation data of Cameron[12] and was therefore was chosen as the empirical model for this thesis:

$$\text{Fume generation rate} = K_3 * O_2{}^x * N_2{}^y * e^{-\Delta E/RT} \tag{33}$$

Here it was assumed that O_2 and N_2 raised to some power would describe the fume generation rate. It was once again assumed that there is an Arrhenius temperature dependence.

The constants in these two equations were determined by using a nonlinear regression analysis program[60]. The final equations for fume generated in the electric furnace (the apparatus used in this thesis) are:

$$\text{Fume gen. (g/min)} = 20.19 * O_2{}^{0.218} * N_2{}^{0.915} * e^{-15690/RT} \tag{34}$$

Parameter, value	Std. dev.
$K_3 = 20.19$	4.52
$x = 0.218$	0.042
$y = 0.915$	0.111
$\Delta E = 15690$ cal/gmole	1350 cal/gmole

$$\text{Fume gen. (g/min)} = 3.33 * \ln(194*O_2) * N_2 * e^{-15695/RT} \tag{35}$$

Parameter, value	Std. dev.
$K_1 = 3.33$	0.72
$K_2 = 194$	29
$\Delta E = 15695$ cal/gmole	1290 cal/gmole

The flow rates are in liters/minute and the temperature is in ^{o}K.

Seventeen data points were used in the regression program to determine the constants; the residual between the calculated point and the actual data point was found for all seventeen points. The sum of squares of the residuals from Eq. 34 was $7.4*10^{-4}$ and from Eq. 35 was $7.2*10^{-4}$; both equations fit the experimental data equally well. Equation 34 was used for this thesis because this form of equation was used successfully in previous work by Cameron. The equation derived for fume generation by Cameron[2] is:

$$\text{Fume gen. (g/min)} = 161 * O_2{}^{0.274} * N_2{}^{0.907} * e^{-20540/RT} \tag{36}$$

These flow rates are also in liters/minute and the temperature is in ^{o}K.

Equation 36 was derived for fume generation in a 5" high induction furnace, not a 24" high electric furnace (see Eq. 34). Equation 34 and Eq. 36, however, yield

the same results (within 5% of each other) in the temperature range of this study. This shows that the oxidative fuming rate is not highly dependent on the reaction system.

GAS TEMPERATURE VS. FUME TEMPERATURE

One concern with fume flowing in a gas phase is whether the fume is at the same temperature as the gas. The melting point of sodium carbonate is 850°C, so sodium carbonate should be a solid below this temperature. By the time the sodium carbonate fume gets to the cooled tube, the gas will be below this temperature. This should also be true for sodium sulfide fume and sodium chloride fume.

The heat flux from a fume particle is given by:

$$Q = \varepsilon\sigma \, (T_d{}^4 - T_w{}^4) + h_c \, (T_d - T_e) \tag{37}$$

Appendix IX gives a sample calculation using this equation. From this calculation, it can be concluded that the temperature of the fume particle is the same as the gas phase temperature and that a 1 μm fume particle should solidify in approximately 10^{-5} seconds after the gas temperature falls below the particle melting point.

PARTICLE GROWTH

Electron micrographs of fume collected from directly above the melt showed fume particles on the filter as large as 5 μm. The question was raised as to whether these particles grew to that size in the gas phase or whether small fume particles deposited on the filter and then fused together to form these larger particles.

Ulrich[48] derived the following formula for the number of particles in a given volume:

$$N = \frac{1}{C_o^{4/5}\left(c_sAt\right)^{6/5}}$$

(38)

This equation shows that the number of particles decreases with time. Once "N" is calculated, particle sizes can be determined by knowing particle concentration (weight/volume) and the density of the particle. If it is assumed that the sticking coefficient, c_s, is 1 and that fume particles are initially of molecular size, then it can be shown that after three seconds in the gas phase (the time needed for the gas to reach the filter):

average particle radius = 0.45 μm

(39)

This matches the experimental value for the particles leaving the reactor.

If the time in the reactor is increased to 50 seconds (the time needed for the gas to reach the top of the apparatus):

average particle radius = 1.4 μm

(40)

Figure 18 shows the theoretically calulated fume particle size in the furnace for 0 to 50 seconds, if the particles grow by continuous agglomeration. A large part of the growth is shown to occur in the first 0.1 seconds; even if the gas phase stayed hot enough for the particles to stick together and bond for the entire residence time, the particles should not grow to be 5 μm. The conclusion is that the particles on the filter must have grown after being captured, or the particles were splashed onto the filter from the bubbling smelt.
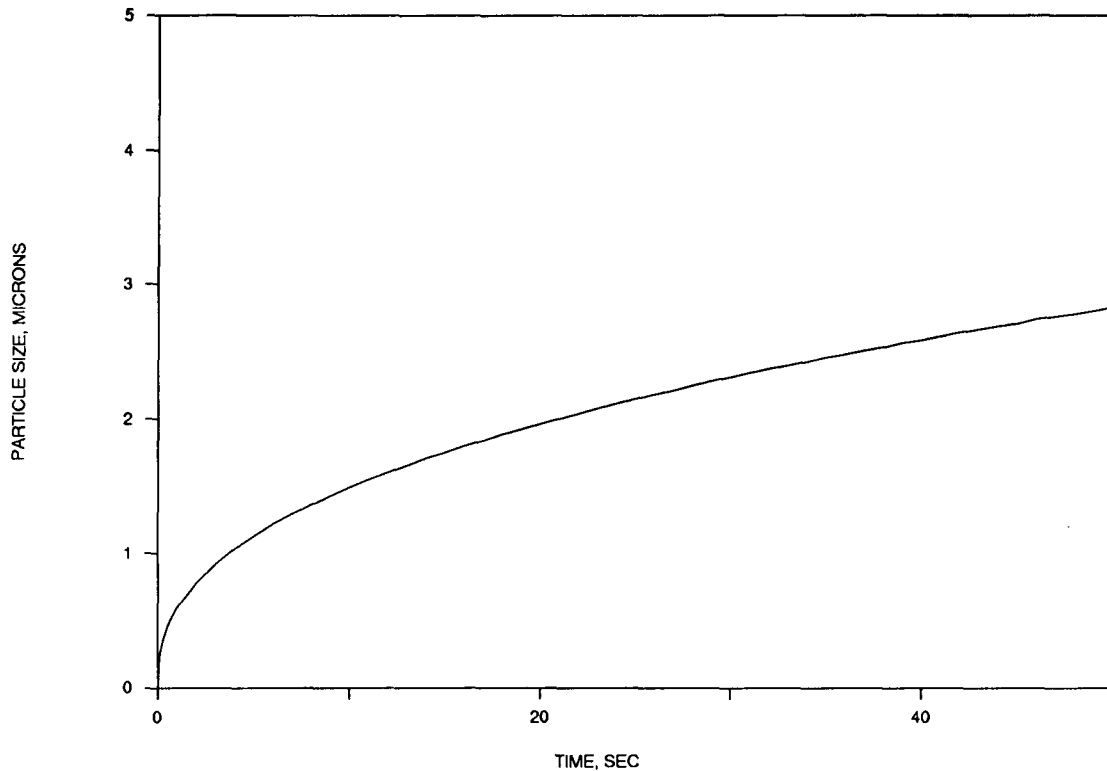
Figure 18. Theoretical particle growth.

TEMPERATURE GRADIENT THROUGH DEPOSITED FUME

As deposits build up on a cooled surface, the rate of heat transfer between the tube coolant and flue gas will change. This will increase the surface temperature of the deposit.

Appendix X shows a sample calculation for the surface temperature increase due to the build-up of deposits on the cooled tubes used in this apparatus. This calculation used the greatest deposit thickness that was encountered in order to determine the maximum temperature difference that would be found. The example shows that the temperature difference through the deposit should never be greater than 3ºC. This is a very small difference and can therefore be neglected.

RESULTS AND DISCUSSION

EFFECTS OF WATER VAPOR

Water vapor in the experimental system was found to affect fume composition; the fume was less Na_2CO_3 and more Na_2SO_4 when water vapor was present. Actual precipitator dust is mostly Na_2SO_4 and depleted in Na_2CO_3[3], which is similar to the experimental results when water vapor is present in the system. Na_2SO_4 could be formed by conversion of Na_2CO_3 fume by SO_2 and O_2, or by direct reactions with smelt. Therefore, in actual recovery boilers where water vapor is always present, more Na_2SO_4 fume than Na_2CO_3 fume will be found.

FUME DEPOSITION

An initial set of experiments determined the total deposition of fume as a function of time. The results from this set of data showed that the total amount of deposited fume is directly proportional to the length of time the tube was in the apparatus. This indicates that the accumulation of collected fume does not influence the deposition rate.

Another set of experiments determined fume deposition as a function of position on the cylinder, at a constant fume generation rate. Na_2CO_3 fume was scraped off the cylinder into two piles corresponding to that collected on the upstream side of the cylinder and that collected on the downstream side (bottom and top, respectively). It was found that the same amount of fume deposited on both the upstream and downstream sides of the tube; examples of this are listed in Table 3. This is one indication that the deposition mechanism could be thermophoresis; deposition by thermophoresis is independent of location at the Reynolds numbers used in this study. Deposition by impaction would produce more deposits on the leading edge.

Table 3. Deposition as a function of location on cylinder.

Gas temperature = 310ºC

Data point	Fume,g Upstream	Downstream
1	0.0053	0.0057
2	0.0165	0.0193
3	0.0215	0.0239
4	0.0229	0.0195
5	0.0207	0.0195

Particle size distributions were obtained for Na_2CO_3, Na_2SO_4, NaCl, and Na_2SO_4/NaCl deposited fume. These distributions were compared to the distributions of the generated fume. It was found that, for Na_2CO_3 fume, the generated fume particles and the deposited fume particles had the same size distribution and the same average size. The same was true for Na_2SO_4 fume particles. No electron micrographs were taken for NaCl generated fume so no comparisons between generated and deposited fume particle sizes could be made. NaCl generated fume particles and deposited fume particles, like Na_2CO_3 and Na_2SO_4 fume, should have the same particle size distribution and the same average particle size.

Na_2CO_3 DEPOSITION

The rate of Na_2CO_3 deposition was found to be proportional to fume concentration (all other variables held constant) and unaffected by gas flow rate (all

other variables held constant). These results are shown in Fig. 19 and Fig. 20, respectively, and match those predicted by thermophoretic theory. The slope of Fig. 20 is 0.0020 ± 0.0025 g min/L, which statistically shows that flow rate has little effect on fume deposition.

Figure 21 shows the dependence of sodium carbonate fume deposition on tube temperature and bulk gas temperature, at a gas flow rate of 5.9 L/min. DEL T is the temperature difference between the bulk flue gas and the surface of the tube; TUBE T is the cooled tube surface temperature. These data points were taken at three different flue gas temperatures: 253°C, 396°C, and 527°C. A straight line through the origin is predicted by thermophoretic theory.

The equation for Fig. 21 is:

$$Na_2CO_3 \text{ dep. (g)} = 0.0959 \left(\frac{\Delta T}{T_w} \right) \tag{41}$$

Dep. time = 15 minutes

Dep. area = 97 cm^2

Fume concentration = 0.0150 g/L

The constant in this equation (0.0959) was calculated by forcing the line through the origin. It can be shown, by statistical methods, that this is valid at 95% confidence (see Appendix XI for the calculation); the intercept is 0.00407 ± 0.00698 g. It can also be shown that, at $\Delta T/T_w=0.5$, a 95% confidence interval for total fume deposited is 0.0479 ± 0.0045 g, which is 9.4% above and below the calculated value of 0.0479 g. This calculation is also shown in Appendix XI.
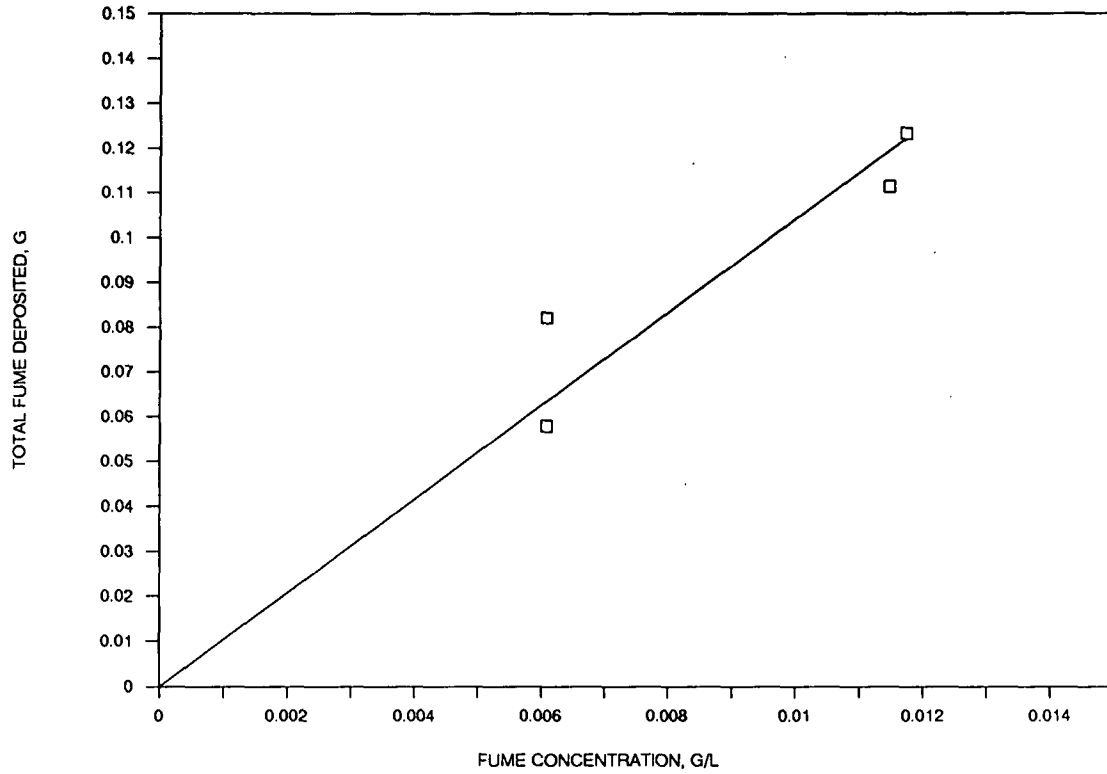
Figure 19. Effect of fume concentration on Na₂CO₃ deposition.

The total model for sodium carbonate deposition is therefore:

$$Na_2CO_3 \text{ dep. rate (g/min/cm}^2) = 0.00440 \text{ C} \left(\frac{\Delta T}{T_w}\right)$$

(42)

where:

C [=] concentration in g/L

T [=] °K

An electron micrograph of deposited Na₂CO₃ fume is shown in Fig. 22. Particles are smooth and spherical, with no sintering between the particles.
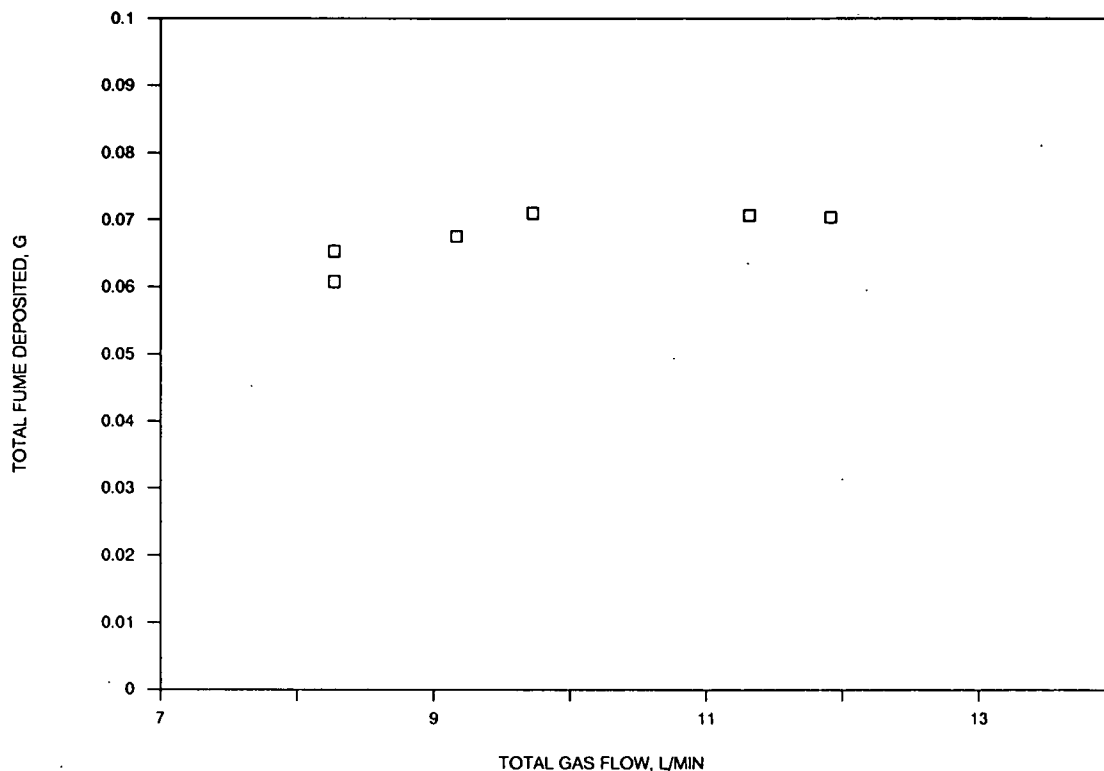
Figure 20. Effect of gas flow on Na_2CO_3 deposition.

Na_2SO_4 DEPOSITION

Figure 23 shows the results of Na_2SO_4 deposition on the cooled tube, at a gas flow rate of 5.8 L/min; data points were taken at two different flue gas temperatures: 238°C and 501°C. This demonstrates that Na_2SO_4, like Na_2CO_3, deposits by thermophoresis. The equation for Fig. 23 is:

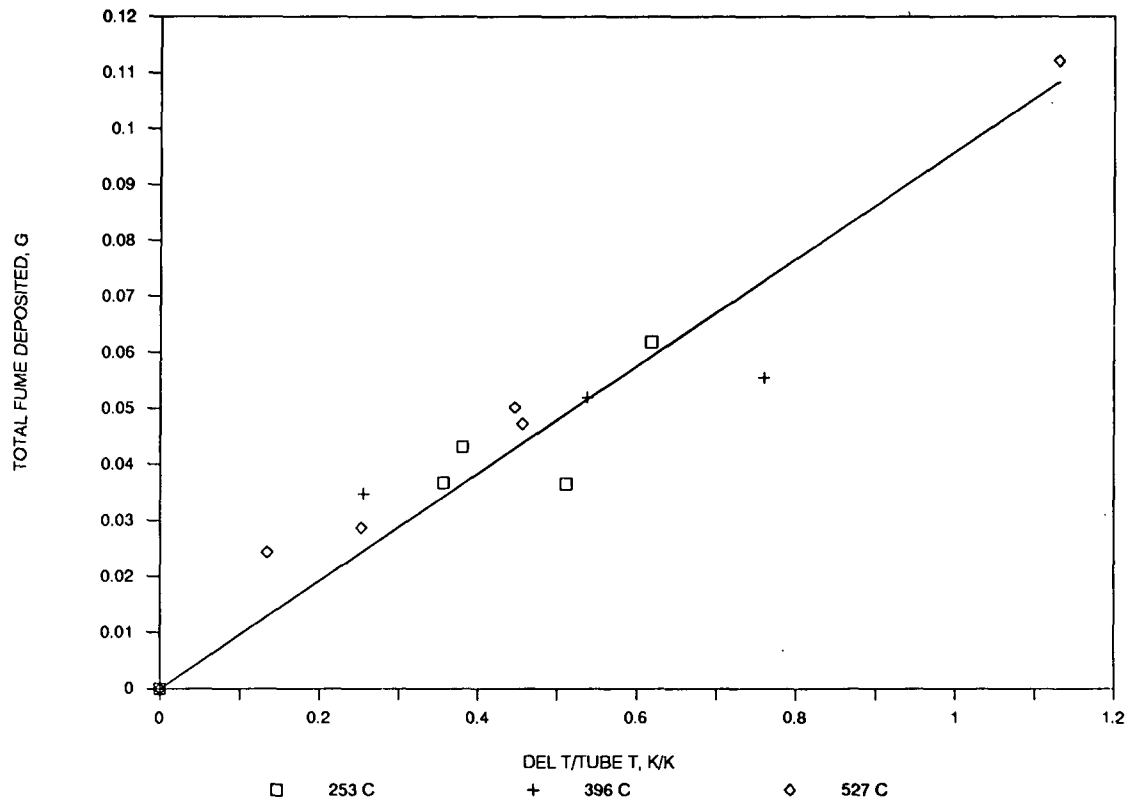$$Na_2SO_4 \text{ dep. (g)} = 0.0964 \left(\frac{\Delta T}{T_w} \right)$$

(43)

Figure 21. Effect of temperature on Na_2CO_3 deposition.

Dep. time = 15 minutes

Dep. area = 97 cm^2

Fume concentration = 0.0158 g/L

As with Na_2CO_3 deposition, the constant (0.0964) was calculated by forcing the line through the origin. This is valid at 95% confidence in this case as well; the intercept is 0.00145$\pm$0.00587 g. At $\Delta T/T_w$=0.5 the total fume deposited is 0.0482$\pm$0.0037 g at a 95% confidence interval, which corresponds to 7.7% above and below the calculated value of 0.0482 g.
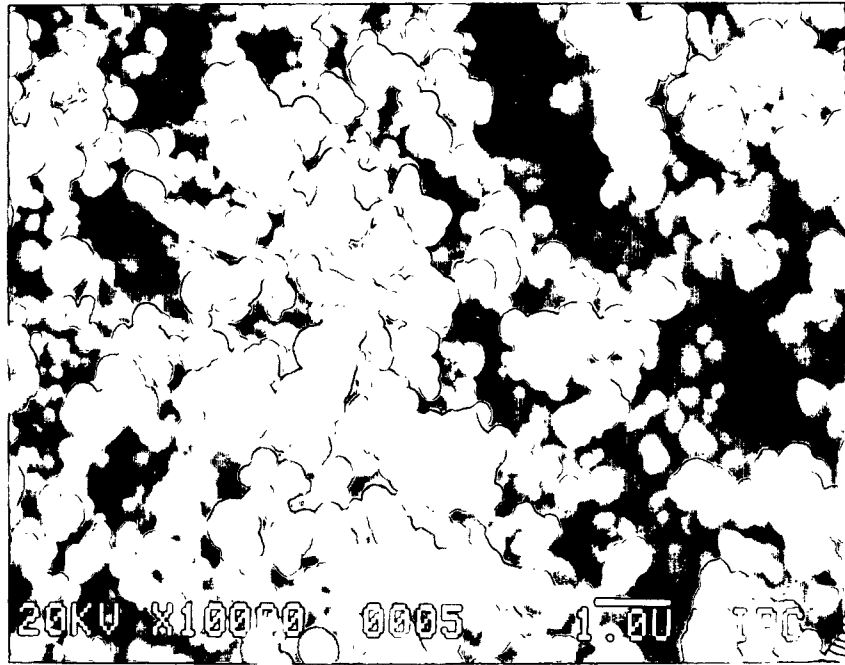
Figure 22. Deposited Na₂CO₃ fume.

Na₂SO₄ particles were produced from Na₂CO₃ fume and look like Na₂CO₃ fume (see Fig. 24). The particles again are smooth and spherical, and no sintering is observed. It was therefore assumed that they act like Na₂CO₃ fume; the deposition rate was assumed to be independent of gas flow rate and proportional to fume concentration. The final equation for Na₂SO₄ deposition is:

$$Na_2SO_4 \text{ dep. rate (g/min/cm}^2) = 0.00419 \, C \left(\frac{\Delta T}{T_w} \right)$$
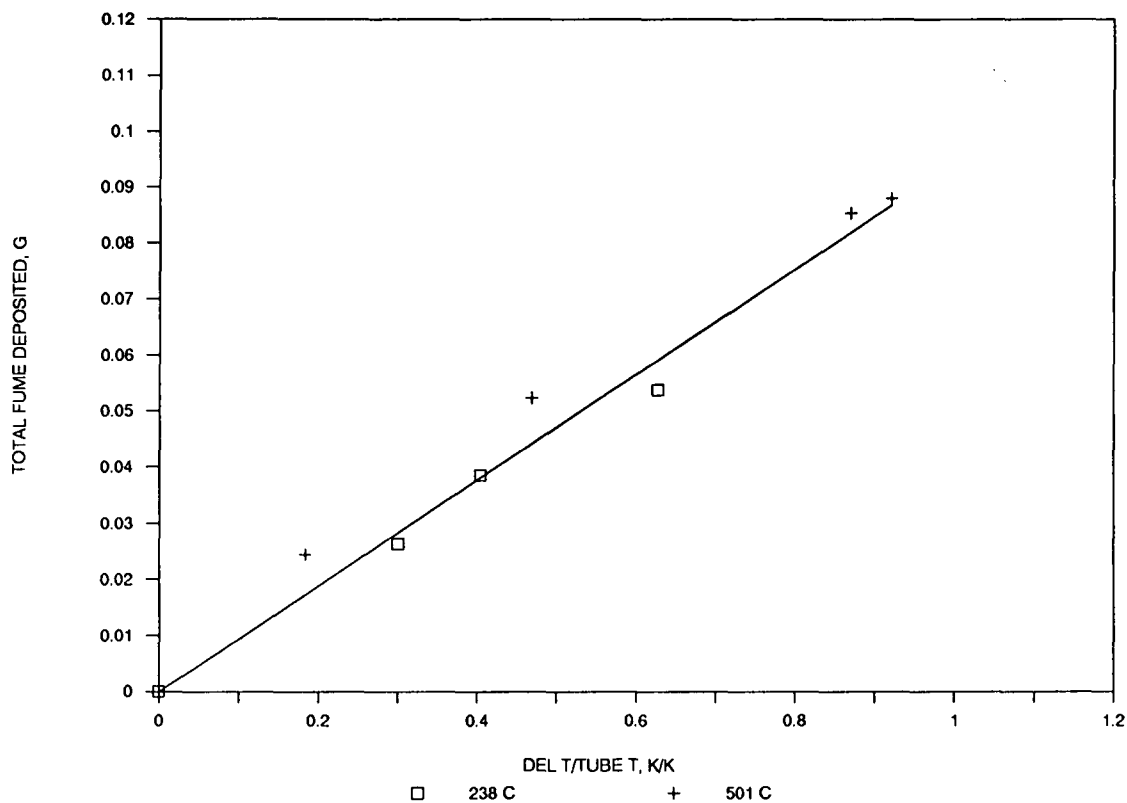
(44)

where:

C [=] g/L

T [=] °K

Figure 23. Effect of temperature on Na₂SO₄ deposition.

NaCl DEPOSITION

The NaCl deposition rate was found to be proportional to fume concentration, as shown in Fig. 25; the deposition rate at a fume concentration of 0.00471 g/L is 3.5 times greater than at 0.00133 g/L. This result was also observed for Na₂CO₃ deposition, and is predicted by thermophoretic theory.

Figure 26 shows that NaCl, like sodium carbonate and sodium sulfate, deposits by thermophoresis but at a much slower rate. These data points were taken at a gas flow rate of 6.0 L/min and at three different flue gas temperatures: 253°C, 369°C, and 520°C. It is assumed that, like Na₂CO₃ and Na₂SO₄ deposition, there is no relation between deposition rate and gas flow rate.
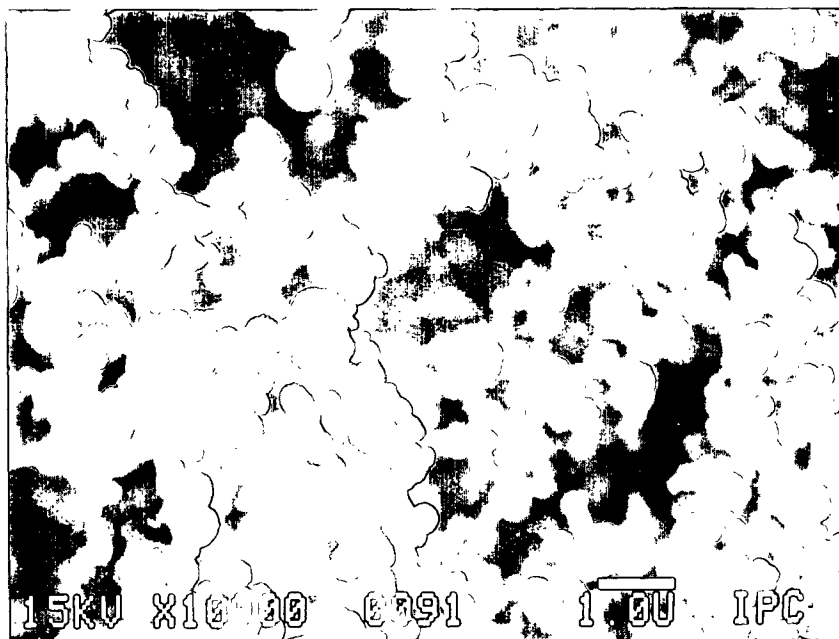
Figure 24. Deposited Na_2SO_4 fume.

The equation for Fig. 26 is:

$$NaCl\ dep.\ (g) = 0.0201 \left(\frac{\Delta T}{T_w}\right)$$

(45)

Dep. time = 30 minutes

Dep. area = 97 cm^2

Fume concentration = 0.00471 g/L

It is once again valid to force the line through the origin; the intercept is 0.000613±0.00233 g at 95% confidence. At $\Delta T/T_w$=0.5, a 95% confidence interval for the amount of fume deposited is 0.0100±0.0013 g, which is 13.0% above and below the calculated value of 0.0100 g.
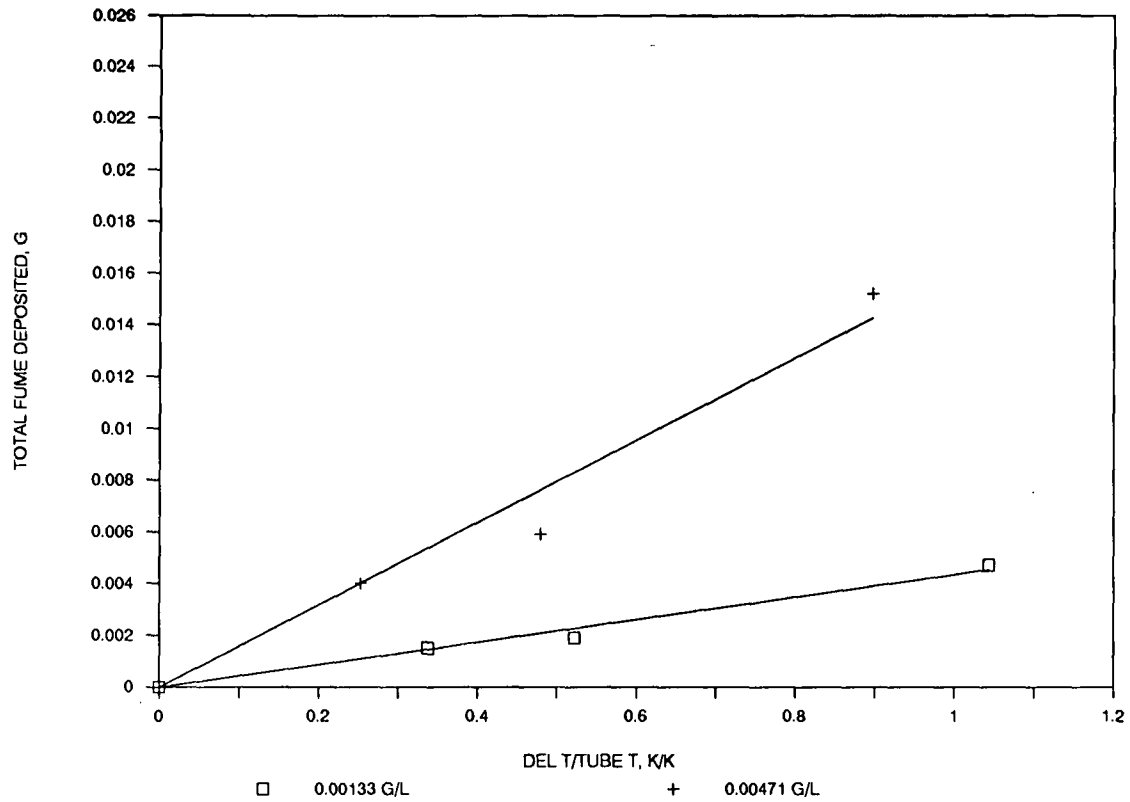
Figure 25. Effect of fume concentration on NaCl deposition.

The final equation, therefore, is:

$$\text{NaCl dep. rate (g/min/cm}^2) = 0.00146 \, C \left(\frac{\Delta T}{T_w} \right)$$

(46)

where:

C [=] g/L

T [=] °K

An electron micrograph of NaCl deposited fume is shown in Fig. 27. This micrograph shows fume particles approximately the same size as Na_2CO_3 fume; however, the NaCl particles show signs of sintering. Sintering was not encountered in either Na_2CO_3 or Na_2SO_4 fume deposition.
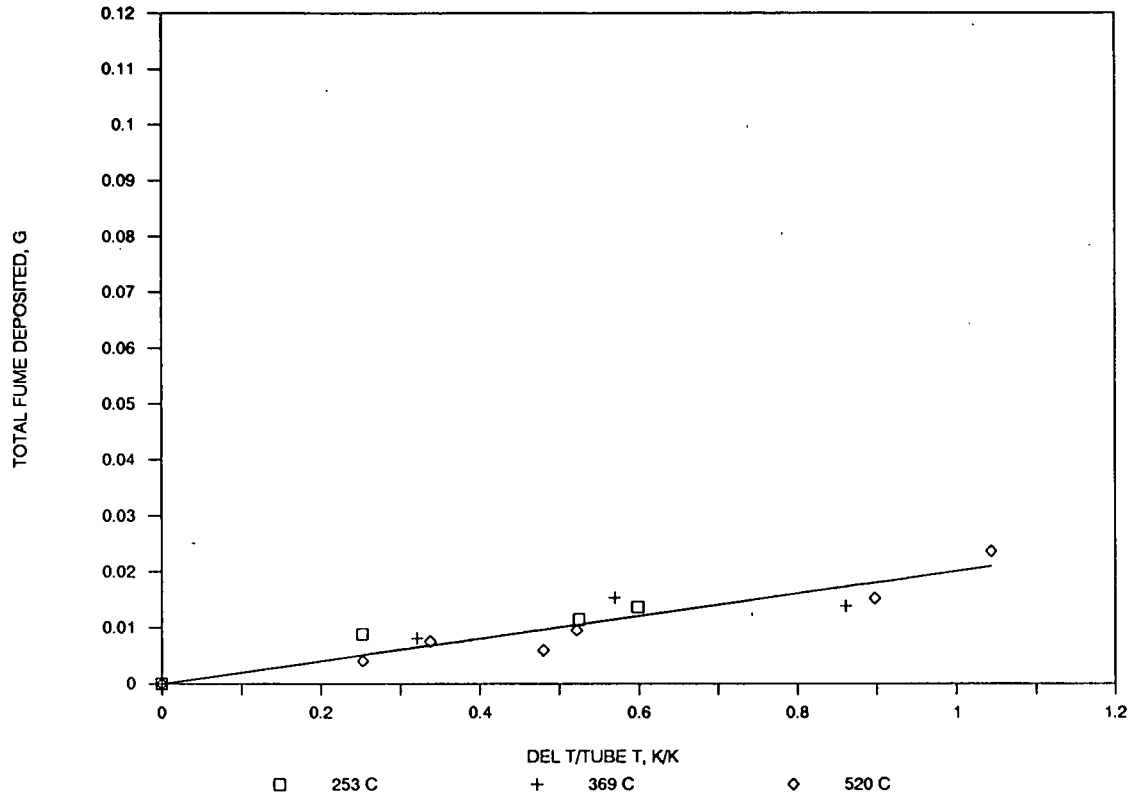
Figure 26. Effect of temperature on NaCl deposition.

Na2SO4/NaCl DEPOSITION

Simultaneous Na2SO4 fume and NaCl fume deposition results are shown in Fig. 28, with flue gas temperatures of 248°C, 374°C, and 524°C. The equation for this graph is:

$$Na_2SO_4/NaCl \text{ dep. (g)} = 0.0824 \left| \frac{\Delta T}{T_w} \right|$$

(47)

Dep. time = 15 minutes

Dep. area = 97 cm^2
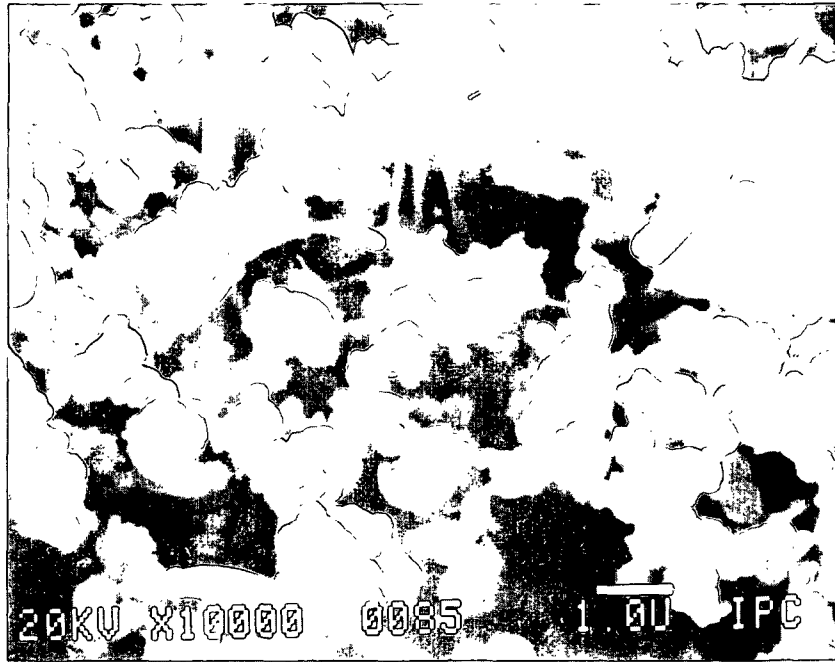
Fume concentration = 0.0205 g/L

Figure 27. Deposited NaCl fume.

The line was forced through the origin; once again this can be shown to be valid. At 95% confidence, the intercept is 0.00506+0.00722 g. The total fume deposited at $\Delta T/T_w$=0.5 is 0.0412+0.0044 g at a 95% confidence interval, which is a spread of 10.7% around the calculated value of 0.0412 g.

It was assumed that the deposition rate is proportional to fume concentration and is independent of flue gas flow rate. The final equation is:

$$Na_2SO_4/NaCl \text{ dep. rate } (g/min/cm^2) = 0.00279 \, C \left(\frac{\Delta T}{T_w} \right) \tag{48}$$

where:

C [=] g/L

T [=] °K
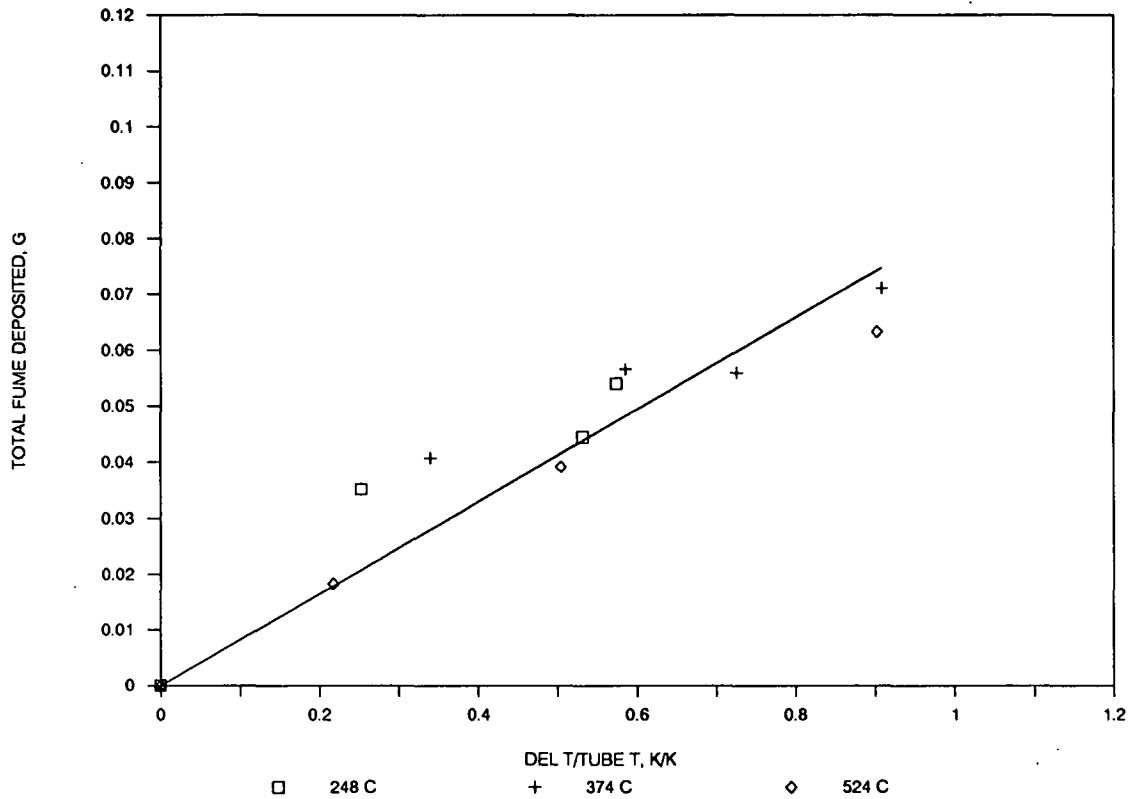
Figure 28. Effect of temperature on Na$_2$SO$_4$/NaCl deposition.

An electron micrograph of Na$_2$SO$_4$/NaCl deposited fume is shown in Fig. 29. Na$_2$SO$_4$/NaCl fume particles are approximately the same size as other fume particles. Some sintering occurred, but not to the extent that pure NaCl fume sintering did.

DEPOSITION RATE COMPARISONS

Table 4 lists all developed rate equations. Rate equations for Na$_2$CO$_3$, Na$_2$SO$_4$, NaCl, and Na$_2$SO$_4$/NaCl deposition by thermophoresis are all of the same form:
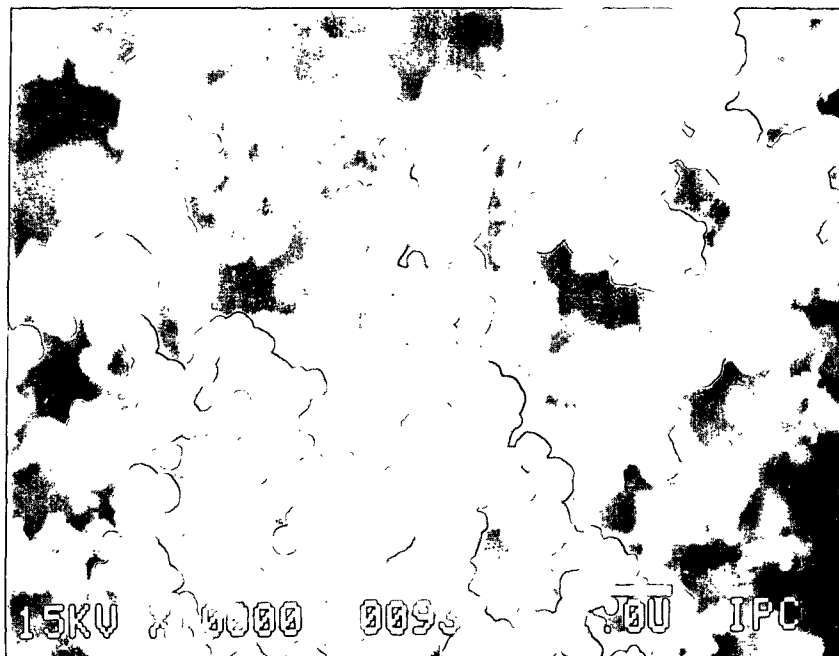
$$\text{Dep. rate} = K\,C \left| \frac{\Delta T}{T_w} \right|$$

(49)

Figure 29. Deposited $Na_2SO_4/NaCl$ fume.

Na_2CO_3 fume and Na_2SO_4 fume, however, deposit at a rate approximately three times faster than $NaCl$ and approximately 1.5 times faster than $Na_2SO_4/NaCl$ fume. The reasons for this are discussed below.

Particle Diameter (d_p)

It was discussed earlier that, in the particle size range of 0.1 µm to 1 µm, the rate of deposition is proportional to diameter. The average deposited particle size for the four fume species, and their variances, are listed in Table 5. These numbers show that Na_2CO_3 fume particles and Na_2SO_4 fume particles are larger than $NaCl$ and $Na_2SO_4/NaCl$ particles and therefore should deposit at a faster rate.

Table 4. Deposition rates by thermophoresis.

$$Na_2CO_3 \text{ dep. rate } (g/min/cm^2) = 0.00440 \, C \left(\frac{\Delta T}{T_w} \right)$$

$$Na_2SO_4 \text{ dep. rate } (g/min/cm^2) = 0.00419 \, C \left(\frac{\Delta T}{T_w} \right)$$

$$NaCl \text{ dep. rate } (g/min/cm^2) = 0.0146 \, C \left(\frac{\Delta T}{T_w} \right)$$

$$Na_2SO_4/NaCl \text{ dep. rate } (g/min/cm^2) = 0.00279 \, C \left(\frac{\Delta T}{T_w} \right)$$

Table 5. Deposited fume particle sizes.

Species	Number avg. diam., μm	95% confidence	Mass avg. diam., μm
Na_2CO_3	0.32	±0.18	0.40
Na_2SO_4	0.29	±0.20	0.42
NaCl	0.21	±0.13	0.27
$Na_2SO_4/NaCl$	0.24	±0.15	0.36

Particle Diffusion Factor (α_T)

It was discussed earlier that the deposition rate in Gokoglu and Rosner's equation is proportional to α_T. Rosner's equations for Na_2SO_4 and NaCl diffusion factors are[39]:

$$\alpha_{T,Na_2SO_4} = 0.78 - \frac{358}{T} \tag{50}$$

$$\alpha_{T,NaCl} = 0.35 - \frac{147}{T} \tag{51}$$

where temperature is in $^\circ$K.

At 500°C,

$$\alpha_{T,Na_2SO_4} = 0.33 \tag{52}$$

$$\alpha_{T,NaCl} = 0.17 \tag{53}$$

The thermal diffusion factor equations for Na_2CO_3 and Na_2SO_4/NaCl were not listed in Rosner's article[39]. However, the thermal diffusion factors for Na_2SO_4 and NaCl show that Na_2SO_4 should deposit faster than NaCl when the particle sizes are the same. This agrees with experimental results.

If α_T and d_p are now separated from the constant in the deposition rate equations (for Na_2SO_4 and NaCl):

$$Na_2SO_4 \text{ dep. rate (g/min/cm}^2) = 0.034\, \alpha_T\, d_p\, C \left(\frac{\Delta T}{T_w} \right) \tag{54}$$

$$NaCl \text{ dep. rate (g/min/cm}^2) = 0.037\, \alpha_T\, d_p\, C \left(\frac{\Delta T}{T_w} \right) \tag{55}$$

The mass average diameter, not the number average diameter, was used to determine these new equations. These two equations are now almost identical. It can be assumed that Na_2CO_3 deposition and $Na_2SO_4/NaCl$ deposition behave similarly. The equations show that the main factors affecting the fume deposition rate are α_T, d_p, C, and $\Delta T/T_w$, and that all fume deposition in the experimental apparatus can be written as:

$$\text{Dep. rate (g/min/cm}^2) = 0.036\ \alpha_T\ d_p\ C\left(\frac{\Delta T}{T_w}\right)$$

(56)

where:

$d_p\ [=]\ \mu m$

$C\ [=]\ g/L$

$T\ [=]\ ^{\circ}K$

EXTRAPOLATION TO RECOVERY BOILER CONDITIONS

An equation derived by Gokoglu and Rosner[29] for thermophoretically augmented mass transfer across laminar boundary layers (0<Re<10,000) is:

$$\text{Dep. rate} = \rho_m\ V\left(\alpha_T\frac{Pr}{Sc}\right)St_h\left(\frac{\Delta T}{T_w}\right)\omega_m$$

(57)

The Stanton number, St_h, can be written as:

$$St_h = \frac{h}{\rho V c_p}$$

(58)

and the ratio of Prandtl to Schmidt numbers is:

$$\frac{Pr}{Sc} = Le$$

(59)

This simplifies Gokoglu and Rosner's equation to:

$$\text{Dep. rate} = \frac{h}{c_p}\left(\alpha_T Le\right)\left(\frac{\Delta T}{T_w}\right)\omega$$

(60)

and shows that the deposition rate is proportional to the heat transfer coefficient.

For air flowing past a single cylinder[61]:

$$\frac{hD}{k} = 0.35 + 0.56(Re)^{0.52}$$

(62)

For the experimental apparatus, the Reynolds number is 2.5, gas conductivity is $1.4*10^{-4}$ cal/cm sec $^\circ$K, and tube diameter is 2.2 cm. The heat transfer coeffieient is calculated to be $7.9*10^{-5}$ cal/cm^2 min $^\circ$K (Pr=1), leading to the following equation derived from Eq. 56:

$$\text{Dep. rate (g/min/cm}^2) = 452\, h\, \alpha_T\, d_p\, C\left(\frac{\Delta T}{T_w}\right)$$

(63)

where:

h [=] cal/cm^2 min $^\circ$K

For air flowing normal to a bank of tubes, a simplified heat transfer equation is[62]:

$$\frac{hD}{k} = 0.3\,(Re)^{0.6}$$

(61)

and boundary layer separation[63] occurs at 110°. For actual recovery boilers, the Reynolds number is approximately 5000, and tube diameter is 6.4 cm. The heat transfer coefficient is calculated to be $1.1*10^{-3}$ cal/cm^2 min $^\circ$K.

Suppose fume deposited equally on the entire surface of the recovery boiler bank tube with the following conditions:

1. Na_2SO_4 fume.

2. $\alpha_T = 0.41$.

3. $d_p = 0.42 \, \mu m$.

4. $C = 0.05 \, g/L$.

5. $T_c = 700^oC$.

6. $T_w = 180^oC$.

The amount of fume that should be deposited, calculated by Eq. 63, is:

$$\text{Dep. rate} = 1.0*10^{-3} \, g/min/cm^2 \tag{62}$$

The actual temperature gradient pattern on the downstream side of the tube, however, is unknown because of boundary layer separation. Therefore, suppose fume only deposits on the upstream side of the tube, when $\phi < 110^o$ (see Fig. 1); fume will then deposit on 220° of the tube or 61% of the tube surface. The fume deposition rate would be 61% of Eq. 62, or:

$$\text{Dep. rate} = 6.1*10^{-4} \, g/min/cm^2 \tag{63}$$

These two numbers bound the fume deposition rate by thermophoresis:

$$6.1*10^{-4} < \text{Dep. rate} < 1.0*10^{-3} \, g/min/cm^2 \tag{64}$$

An actual fume deposition rate at the boiler bank inlet[1] under similar conditions is:

$$\text{Dep. rate} = 6.7*10^{-4} \, g/min/cm^2 \tag{65}$$

which is within the calculated bounds for fume deposition by thermophoresis. This shows that thermophoresis is a main mechanism of fume deposition in a recovery boiler.

If some fume particles in a recovery boiler agglomerate to sizes as great or greater than 10 μm, deposition by particle impaction is still possible. Agreement between caclulated thermophoretic deposition rates and actual deposition rates, however, show that this is unlikely.

RECOVERY BOILER DESIGN IMPLICATIONS

There is one main reason for determining the mechanisms responsible for fume deposition in a recovery boiler: know the controlling parameters and therefore have the ability to affect the deposition rate by changing these parameters.

Thermophoresis is the main mechanism for fume deposition in recovery boilers; its controlling parameters are flue gas temperature, tube surface temperature, particle composition and size, particle concentration, and (to some extent) gas flow rate. It is impossible to change any one variable without affecting other boiler operating conditions. For instance, increasing the tube temperature will result in less fume deposition but the flue gas will be cooled less. Knowledge gained from these experimental results may be difficult to impliment in an existing recovery boiler; it would best be used in the design of new furnaces.

CONCLUSIONS

This thesis has shown that thermophoresis is the main deposition mechanism for fume particles under the following experimental conditions:

1. Fume particle sizes from 0.1 μm to 1 μm in diameter.

2. Flue gas temperatures from 250°C to 580°C.

3. Reynolds numbers less than 3 (based on cooled tube diameter).

The following equations were derived:

$$Na_2CO_3 \text{ dep. rate (g/min/cm}^2) = 0.00440 \, C\left(\frac{\Delta T}{T_w}\right) \tag{66}$$

$$Na_2SO_4 \text{ dep. rate (g/min/cm}^2) = 0.00419 \, C\left(\frac{\Delta T}{T_w}\right) \tag{67}$$

$$NaCl \text{ dep. rate (g/min/cm}^2) = 0.0146 \, C\left(\frac{\Delta T}{T_w}\right) \tag{68}$$

$$Na_2SO_4/NaCl \text{ dep. rate (g/min/cm}^2) = 0.00279 \, C\left(\frac{\Delta T}{T_w}\right) \tag{69}$$

where:

C [=] g/l

T [=] °K

It was also found that, during simultaneous $Na_2SO_4/NaCl$ generation, the generation of Na_2SO_4 and the generation of NaCl were additive and independent. The simultaneous deposition of the two compounds, however, were not independent of each other.

The general equation for fume deposition in this thesis is:

$$\text{Dep. rate} = K\,\alpha_T\,d_p\,C\left|\frac{\Delta T}{T_w}\right| \tag{70}$$

which closely resembles Gokoglu and Rosner's equation:

$$\text{Dep. rate} = \frac{h}{c_p}\left(\alpha_T\,Le\right)\left(\frac{\Delta T}{T_w}\right)\omega \tag{71}$$

The following conditions were used to obtain the experimental result:

1. Fume particle sizes from 0.1 μm to 1 μm.

2. Flue gas temperatures from 250°C to 580°C.

3. Reynolds numbers less than 3, based on cooled tube diameter.

Other important results are:

1. Gas flow rate has little effect on the deposition rate.

2. The fume deposition rate is the same on the upstream and downstream side of the cooled cylinder.

3. No fume deposition occurs when no temperature gradient is present.

4. The accumulation of collected fume does not influence the deposition rate.

These results are directly applicable to fume deposition in the generating bank and the economizer section in recovery boilers, where flue gas temperatures range from 200°C to 700°C. The Reynolds number in a boiler bank is between 3000 and 5000; the heat transfer coefficient is a function of Reynolds number and the deposition rate is proportional to the heat transfer coefficient. If the difference in flow rate between the experimental system and the recovery boiler is taken into account, the experimental results show close agreement with actual recovery boiler data.

If some fume particles in a recovery boiler agglomerate to sizes as great or greater than 10 μm, deposition by particle impaction is still possible. Agreement between caclulated thermophoretic deposition rates and actual deposition rates, however, show that this is unlikely.

Water vapor in the system was found to affect the fume composition; fume composition was less Na_2CO_3 and more Na_2SO_4 when water vapor was present.

RECOMMENDATIONS

Two future research possibilities arise from this thesis. First, determine, in greater detail, the reactions of water vapor and fume. This is important because the composition of the fume has an effect on the deposition rate.

Second, repeat the experiments at a Reynolds number closer to that found in a recovery boiler (approximately 5000). This will experimentally determine the effects of boundary layer regimes. Changes would have to be made to the apparatus, because the present construction of this apparatus limits the gas flow rates. Changes may be difficult to accomplish. Adding fans above the melt but below the cooled tube would increase the gas flow rate but would drastically decrease the fume concentration; increasing the gas flow through the melt would result in much bubbling and splashing from the smelt.

ACKNOWLEDGEMENTS

LITERATURE CITED

1.   Weyerhaeuser Company, Federal Way, WA, 1986.

2.   Cameron, J. H. Fume generation in kraft recovery boilers. PIMA: 32-34 March 1986)

3.   Tran, H. N. How does a recovery boiler become plugged? 1986 Recovery Operations Seminar Proceedings: 145-153.

4.   Reeve, D. W.; Tran, H. N.; Barham, D. Superheater fireside deposits and corrosion in kraft recovery boilers. Tappi 64(5): 109-113 (May 1981).

5.   Reeve, D. W.; Tran, H. N.; Barham, D. The effluent-free bleached kraft pulp mill - Part IV: Morphology, chemical, and thermal properties of recovery boiler superheater fireside deposits. Pulp and Paper Canada 82(9): 105-110 (September 1981).

6.   Tran, H. N. Formation of kraft recovery boiler superheater fireside deposits. 1981 International Conference on Recovery of Pulping Chemicals Proceedings: 119-125.

7.   Tran, H. N.; Reeve, H. N.; Barham, D. Formation of kraft recovery boiler superheater fireside deposits. Pulp and Paper Canada 84(1): 36-41 (1983).

8.   Tran, H. N.; Reeve, D. W. Kraft recovery unit fireside deposits and plugging. Pulp and Paper Canada 85(10): 54-57 (1984).

9.   Tran, H. N.; Reeve, D. W.; Barham, D. Local reducing atmosphere - a significant cause of superheater corrosion in kraft recovery units. 1984 Tappi Engineering Conference Proceedings: 73-77.

10.   Isaak, P.; Tran, H. N.; Barham, D.; Reeve, D. W. Stickiness of fireside deposits in kraft recovery units: Part II. The effects of potassium and surface treatment. Presented at the CPPA Annual Meeting, January 1987.

11.   Bosch, J.C.; Pilat, M. J.; Hrutfiord, B. F. Size distributions of aerosols from a kraft mill recovery furnace. Tappi 54(11): 1871-1875 (November 1971).

12.   Cameron, J. H.; Clay, D. T.; Grace, T. M. Oxidative fuming - the phenomenon and possible interpretations. 1985 Tappi International Chemical Recovery Conference Proceedings: 435-444.

13.   Blackwell, B.; King, T. Technology review: exploring kraft recovery boiler chemical reactions. Pulp and Paper 59(11): 122-124 (November 1985).

14. Cameron, J. H. Vaporization from alkali carbonate melts with reference to the kraft recovery furnace. Journal of Pulp and Paper Science 14(4): J76-J81 (July 1988).

15. Brown, T. D. The deposition of sodium sulfate from combustion gases. Journal of the Institute of Fuel 39: 378-385 (1966).

16. Reid, W. T. External Corrosion and Deposits - Boilers and Gas Turbines. American Elsevier Publishing Company, Inc., 1971.

17. Schlichting, H. Boundary Layer Theory. McGraw-Hill Book Company, 1955.

18. Fuchs, N. A. The Mechanics of Aerosols. The Macmillan Company, 1964: 107-180.

19. Reference 11 in Wood, N. B. The mass transfer of particles and acid vapor to cooled surfaces. Journal of the Institute of Energy 54(6): 76-93 (June 1981).

20. Davies, C. N. Aerosol Science. Academic Press, 1966.

21. Friedlander, S. K.; Johnstone, H. F. Deposition of suspended particles from turbulent gas streams. Industrial and Engineering Chemistry 49(7): 1151-1156 (July 1957).

22. Wood, N. B. The mass transfer of particles and acid vapor to cooled surfaces. Journal of the Institute of Energy 54(6): 76-93 (June 1981).

23. Tran, H. N.; Reeve, D. W.; Barham, D. Formation of kraft recovery boiler superheater fireside deposits. Pulp and Paper Canada 84(1): 36-41 (1983).

24. Fuchs, N. A. The Mechanics of Aerosols. The Macmillan Company, 1964: 57-69.

25. Cawood, W. The movement of dust or smoke particles in a temperature gradient. Trans. Farad. Soc. 32: 1068-1073 (1936).

26. Referenced in Raask, E. Mineral Impurities in Coal Combustion. Hemisphere Publishing Corporation, 1985: 191.

27. Wessel, R. A.; Wagoner, C. L. Ash deposits - initiating the change from empiricism to generic engineering - Part 2: Initial results. Presented at the Jt. ESME/IEEE Power Generation Conference, Portland, Oregon (October 1986).

28. Walker, K. L.; Homsy, G. M.; Geyling, F. T. Thermophoretic deposition of small particles in laminar tube flow. Journal of Colloid and Interface Science 69(1): 138-147 (March 1979).

29. Gokoglu, S. A.; Rosner, D. E. Thermally augmented mass transfer rates to solid walls across laminar boundary layers. AIAA Journal: 172-179 (January 1986).

30. Gokoglu, S. A.; Rosner, D. E. Correlation of thermophoretically-modified small particle diffusional deposition rates in forced convection systems with variable properties, transpiration cooling and/or viscous dissipation. Int. J. Heat Mass Transfer 27(5): 639-646 (1984).

31. Cussler, E. L. Diffusion, Mass Transfer in Fluid Systems. Cambridge University Press, 1984.

32. Kohl, F. J.; Santoro, G. J.; Stearns, C. A.; Fryburg, G. C.; Rosner, D. E. Theoretical and experimental studies of the deposition of Na_2SO_4 from seeded combustion gases. J. Electrochem. Soc.: Solid-State Science and Technology: 1054-1061 (June 1979).

33. Rosner, D. E.; Chen, B. K.; Fryburg, G. C.; Kohl, F. J. Chemically frozen multicomponent boundary layer theory of salt and/or ash deposition rates from combustion gases. Combustion Science and Technology 20: 87-106 (1979).

34. Vermes, G. Thermophoresis - enhanced deposition rates in combustion turbine blade passages. Transactions of the ASME: Journal of Engineering for Power: 542-548 (October 1979).

35. Goren, S. L. Thermophoresis of aerosol particles in the laminar boundary layer on a flat plate. Journal of Colloid and Interface Science 61(1): 77-85 (August 1977).

36. Homsy, G. M.; Geyling, F. T.; Walker, K. L. Blasius Series for thermophoretic deposition of small particles. Journal of Colloid and Interface Science 83(2): 495-501 (October 1981).

37. Derjaguin, B. V.; Rabinovich, YA. I.; Storozhilova, A. I.; Shcherbina, G. I. Measurement of the coefficient of thermal slip of gases and the thermophoretic velocity of large-size aerosol particles. Journal of Colloid and Interface Science 57(3): 451-461 (December 1976).

38. Rosenblatt, P.; LaMer, V. K. Motion of a particle in a temperature gradient; Thermal repulsion as a radiometer phenomenon. Phys. Rev. 70: 385-395 (1946).

39. Rosner, D. E. Thermal (Soret) diffusion effects on interfacial mass transport rates. PhysicoChemical Hydrodynamics 1: 159-185 (1980).

40. Rosner, D. E.; Liang, B. Laboratory studies of the deposition of alkali sulfate vapors from combustion gases using a flash-evaporation technique. Chem. Eng. Commun. 42: 171-196 (1986).

41. Raask, E. Reactions of coal impurities during combustion and deposition of ash constituents on cooled surfaces. The Mechanism of Corrosion by Fuel Impurities. London, Butterworths, 1963: 145-153.

42. Bishop, R. J. The formation of alkali-rich deposits by a high-chlorine coal. Journal of the Institute of Fuel 41(2): 51-65 (February 1968).

43. Bishop, R. J.; Cliffe, K. R. Condensation of sodium chloride from a moving gas stream. Journal of the Institute of Fuel: 3-5 (July 1969).

44. Seshadri, K.; Rosner, D. E. Optical methods and results of dew point and deposition rate measurements in salt/ash-containing combustion gases - $B_2O_3(l)$ deposition rates by interference methods and comparisons with theory. AIChE Journal 30(2): 187-196 (March 1984).

45. Bishop, R. J.; Cliffe, K. R. Condensation behaviour of sodium chloride during convective heat transfer. Journal of the Institute of Fuel 39(7): 441-448 (November 1970).

46. Ulrich, G. D.; Subramanian, N. S. Particle growth in flames - III. Coalescence as a rate controlling process. Combustion Science and Technology 17: 119-126 (1977).

47. Ulrich, G. D. Theory of particle formation and growth in oxide synthesis flames. Combustion Science and Technology 4: 47-57 (1971).

48. Ulrich, G. D. Flame systhesis of fine particles. Chemical & Engineering News: 22-29 (August 6, 1984).

49. Ulrich, G. D.; Reihl, J. W. Aggregation and growth of submicron oxide particles in flames. Journal of Colloid and Interface Science 87(1): 257-265 (May 1982).

50. Medalia, A. I.; Heckman, F. A. Morphology of aggregates - II. Size and shape factors of carbon black aggregates from electron microscopy. Carbon 7: 567-582 (1969).

51. Weaver, A. B.; Johnson, D. L.; St. Pierre, G. R. Thermodynamic computation of phase equilibria in the sodium-carbon-oxygen system. Metallurgical Transactions A 8A: 603-607 (April 1977).

52. Motzfeldt, K. The thermal decomposition of sodium carbonate by the effusion method. Journal of Physical Chemistry 59: 139-147 (February 1955).

53.   Andresen, R. E. Solubility of oxygen and sulfur dioxide in molten sodium sulfate and oxygen and carbon dioxide in molten sodium carbonate. Journal of the Electrochemical Society: Solid-State Science and Technology: 328-334 (February 1979).

54.   Rosner, D. E.; Kim, S. S. Optical experiments on thermophoretically augmented submicron particle deposition from "dusty" high temperature gas flows. Chemical Engineering Journal 29: 147-157 (1984).

55.   Rosner, D. E. Transport Processes in Chemically Reacting Flow Systems. Butterworth Publishers, 1986.

56.   Raask, E. Mineral Impurities in Coal Combustion. Hemisphere Publishing Corporation, 1985.

57.   Maule, G. P. A-190 Independent Study, The Institute of Paper Chemistry, Appleton, WI, 1988.

58.   Cameron, J. H. James River Corporation, Neenah, WI, Personal communication, 1988.

59.   Cameron, J. H. Reaction enhanced vaporization of molten salt. Chem. Eng. Comm. (59): 243-257 (1987).

60.   Dye, J. L.; Nicely, V. A., J. Chem. Education (48), 443 (1971).

61.   McCabe, W. L.; Smith, J. C. Unit Operations of Chemical Engineering. McGraw-Hill Book Company, 1976: 337.

62.   Prabhudesai, R. K.; Das, D. K. Chemical Engineering for Professional Engineering Examinations. McGraw-Hill Book Company, 1984: 98.

63.   Schlichting, H. Boundary Layer Theory. McGraw-Hill Book Company, 1955.

APPENDIX I. SYMBOL DEFINITIONS

A = collision constant

c = constant depending on particle size and shape

c_s = sticking coefficient

C = concentration of fume in flue gas

C_o = number of molecules/cm^3

d_p = particle diameter

D = cylinder diameter

D_v = Brownian diffusion coefficient

ΔE = activation energy

h = heat transfer coefficient

j'' = diffusional mass flux of small particles

k = thermal conductivity

k_m = gas constant for one molecule

K = constant

l_i = stop distance of particle

N = number of particles/cm^3

Nu = Nusselt number

$P_{NaCl(T)}$ = equilibrium partial pressure of NaCl at temperature T

$p^*_{NaCl(T)}$ = vapor pressure of NaCl and temperature T

Pr = Prandtl number

Q = heat flux

R = gas constant

Sc = Schmidt number

St_h = Stanton number for heat transfer

Stk = Stokes number

t = time

T = absolute temperature

v_T = thermophoretic velocity

V = velocity parallel to wall

$\bar{x}$ = displacement in time t

X_{NaCl} = mole fraction of NaCl in the melt

y = direction perpendicular to the wall

α_T = thermal diffusion factor

ε = emissivity

λ_o = molecular mean free path

μ = viscosity of gas

υ = kinematic viscosity

ρ = density

σ = Stefan-Boltzmann constant

ω = mass fraction of particles in mixture

SUBSCRIPTS

e = mainstream

m = outer edge of the Brownian diffusion boundary layer

o = normal temperature and pressure

p = particle

w = wall

APPENDIX II. FURNACE SPECIFICATIONS

ATS, Inc.

Series 3110, Tube Type Laboratory Furnace

6" i.d., 14" o.d., 24" heated length, 28" outside length

1 zone

8400 Watts

230 Volts

Kanthal AL embedded elements for service to 1204°C

Type K thermocouples

APPENDIX III. FILTERING MATERIAL

Gaskets, Inc.

G/I-83 Ceramic Paper

For use up to 1260°C

0.040" thick, 6% binder

It was noticed that, when the paper with binder was introduced into a high temperature environment, the paper would burst into flames and the organic binder would burn. The volatilization of the binder also changed the weight of the paper. For this reason, the paper was heated in a muffle furnace at 950°C for 10 minutes. This eliminated the binder before the paper was used in the experimental apparatus as a filtering material. Lack of binder did not noticeably affect the strength of the paper.

APPENDIX IV. ELECTRIC HEATER SPECIFICATIONS

Watlow Electric Manufacturing Company

Ceramic Fiber Heaters, Semi-cylindrical, Unit number VS406J06S, Style A

For use up to 1093°C

6 $1/2$" i.d., 10 $1/2$" o.d., 6" length

750 Watts

120 Volts

APPENDIX V. Na_2CO_3 DATA

TEMPERATURE EFFECTS

Melt temperature = 950°C

Deposition time = 15 minutes

Fume concentration = 0.0150 g/L

N_2+CO_2 flow rate = 5.9 L/min

Gas T, °K	Tube T, °K	$\Delta T/T_w$	Fume wt, g
526	325	0.618	0.0618
526	381	0.381	0.0431
526	388	0.356	0.0367
526	348	0.511	0.0365
526	526	0	0
669	533	0.255	0.0347
669	435	0.538	0.0519
669	380	0.761	0.0555
669	669	0	0
788	629	0.253	0.0286
788	545	0.446	0.0501
818	562	0.456	0.0472
818	384	1.130	0.1122
818	721	0.135	0.0242
818	818	0	0

CONCENTRATION EFFECTS

Melt temperature = 950°C

Deposition time = 15 minutes

N_2 flow rate below melt = 5.37 L/min

$\Delta T/T_w = 1.7$

N_2 above melt, L/min	CO_2 above melt, L/min	Fume conc., g/L	Fume wt, g
0	3	0.0069	0.0821
0	3	0.0069	0.0578
2	1	0.0115	0.1114
2.5	0.5	0.0117	0.1233

FLOW RATE EFFECTS

Melt temperature = 950°C

Deposition time = 15 minutes

Fume concentration = 0.0150 g/L

N_2 flow rate below melt = 5.37 L/min

$\Delta T/T_w = 0.65$

N_2 above melt, L/min	CO_2 above melt, L/min	Total flow, L/min	Fume wt, g
0	2.9	8.27	0.0608
0.898	2.9	9.12	0.0675
1.45	2.9	9.72	0.0710
3.04	2.9	11.32	0.0707
3.65	2.9	11.92	0.0704
0	2.9	8.27	0.0653

APPENDIX VI. Na_2SO_4 DATA

TEMPERATURE EFFECTS

Melt temperature = 950°C

Deposition time = 15 minutes

Fume concentration = 0.0158 g/L

N_2+SO_2 flow rate = 5.8 L/min

Gas T, °K	Tube T, °K	$\Delta T/T_w$	Fume wt, g
511	393	0.300	0.0262
511	364	0.404	0.0385
511	314	0.627	0.0537
511	511	0	0
774	654	0.183	0.0244
774	527	0.469	0.0523
774	414	0.870	0.0853
774	403	0.921	0.0880
774	774	0	0

APPENDIX VII. NaCl DATA

TEMPERATURE EFFECTS

Melt temperature = 950°C

Deposition time = 30 minutes

Fume concentration = 0.00471 g/L

N_2 flow rate = 6.0 L/min

Gas temp, °K	Tube temp, °K	$\Delta T/T_w$	Fume wt, g
526	420	0.252	0.0088
526	345	0.525	0.0114
526	329	0.599	0.0136
526	526	0	0
642	486	0.321	0.0081
642	409	0.570	0.0153
642	345	0.861	0.0138
642	642	0	0
793	536	0.479	0.0059
793	633	0.252	0.0040
793	418	0.897	0.0152
793	593	0.337	0.0075
793	521	0.522	0.0095
793	388	1.044	0.0235
793	793	0	0

CONCENTRATION EFFECTS

Melt temperature = 950°C

Deposition time = 30 minutes

Fume conc., g/L	Gas T, °K	Tube T, °K	$\Delta T/T_w$	Fume wt, g
0.00133	793	593	0.337	0.0015
0.00133	793	521	0.522	0.0019
0.00133	793	388	1.044	0.0047
0.00133	793	793	0	0
0.00471	793	536	0.579	0.0059
0.00471	793	633	0.253	0.0040
0.00471	793	418	0.897	0.0152
0.00471	793	793	0	0

APPENDIX VIII. $Na_2SO_4/NaCl$ DATA

TEMPERATURE EFFECTS

Melt temperature = 950°C

Deposition time = 15 minutes

Fume concentration = 0.0205 g/L

     (0.0158 g/L Na_2SO_4)

     (0.00471 g/L NaCl)

N_2+SO_2 flow rate = 5.79 L/min

Gas T, °K	Tube T, °K	$\Delta T/T_w$	Fume wt, g
521	416	0.252	0.0352
521	340	0.532	0.0445
521	331	0.574	0.0541
521	521	0	0
647	483	0.340	0.0408
647	408	0.586	0.0566
647	339	0.909	0.0711
647	375	0.725	0.0560
647	647	0	0
797	655	0.217	0.0183
797	530	0.504	0.0392
797	419	0.902	0.0633
797	797	0	0

APPENDIX IX. PARTICLE TEMPERATURE

Calculations to predict the length of time needed for a fume particle to solidify in the gas phase by heat flux from the particle to the gas.

$$Q = \varepsilon\sigma (T_d^4 - T_w^4) + h_c (T_d - T_e) \tag{72}$$

$$\varepsilon = 0.9 \text{ (assumed emmisivity)} \tag{73}$$

$$\sigma = 1.73*10^{-9} \text{ Btu/hr ft}^2 \text{ }^o R \tag{74}$$

$$T_d = 1910^o F \text{ (assumed drop temperature)} \tag{75}$$

$$T_w = 1000^o F \text{ (assumed tube temperature)} \tag{76}$$

$$T_e = 1550^o F \text{ (assumed gas temperature)} \tag{77}$$

$$h_c = Nu * (k_g/d) \tag{78}$$

$$Nu = 2 + 0.51 \text{ Re}^{0.5} \text{ (for a spherical particle)} \tag{79}$$

$$Re = dV\rho/\mu \tag{80}$$

$$V = \text{settling velocity in Stokes law region}$$
$$= gd^2\rho/18\mu \tag{81}$$

$$g = 32.17 \text{ ft/sec}^2 \tag{82}$$

$$d = 1 \text{ } \mu m \text{ (particle diameter)} \tag{83}$$

$$\rho = 118 \text{ lb/ft}^3 \text{ (gas density)} \tag{84}$$

$$\mu = 2.68*10^{-5} \text{ lb/ft sec (gas viscosity)} \tag{85}$$

$$V = 8.5*10^{-5} \text{ ft/sec} \tag{86}$$

$$Re = 2.1*10^{-7} \tag{87}$$

$$Nu = 2.00 \tag{88}$$

$$k_g = [c_p + (5R/4M)]\mu \quad \text{(assume for } N_2 \text{ at } 1550^\circ F) \tag{89}$$

$$c_p = 7.28 \text{ Btu/mole } ^\circ R \text{ (for nitrogen)} \tag{90}$$

$$R = \text{gas constant} \tag{91}$$

$$M = \text{molecular weight (for nitrogen)} \tag{92}$$

$$k_g = 3.37*10^{-2} \text{ Btu/ft hr } ^\circ R \tag{93}$$

$$h_c = 2.05*10^4 \text{ Btu/ft}^2 \text{ hr } ^\circ R \tag{94}$$

$$Q = 7.42*10^6 \text{ Btu/hr ft}^2 \tag{95}$$

Time required to solidify droplet:

$$t = (mc_p\Delta T + m\lambda)/QA \tag{96}$$

$$m = 2.42*10^{-15} \text{ lb (mass of drop)} \tag{97}$$

$$c_p = 0.45 \text{ Btu/lb } ^\circ R \text{ (specific heat of drop)} \tag{98}$$

$$\Delta T = 360^\circ F \tag{99}$$

$$\lambda = 110 \text{ Btu/lb (heat of fusion)} \tag{100}$$

$$A = 8.5*10^{-12} \text{ ft}^2 \text{ (area of drop)} \tag{101}$$

$$t = 1.0*10^{-8} \text{ hr} = 3.6*10^{-5} \text{ sec} \tag{102}$$

APPENDIX X. TEMPERATURE GRADIENT ACROSS FUME

Calculations to determine the difference in temperature between the tube metal surface and the fume surface exposed to the flue gas.

$$T_o\text{-}T_1 = -q_o\left(\frac{x_o\text{-}x_1}{k}\right)$$

(103)

$T_1 = 111.3°C$ (wall temperature) (104)

$q_o = 40,000$ Btu/hr ft^2 (assumed heat flux) (105)

$x_o\text{-}x_1 = 9.30*10^{-4}$ cm (fume thickness assuming 50% porosity) (106)

$$k_{comp} = k_{fume}\left[\frac{\upsilon p^{2/3}+1\text{-}p^{2/3}}{\upsilon\left(p^{2/3}\text{-}p\right)+1\text{-}p^{2/3}+p}\right]$$

(107)

$k_{fume} = 0.5$ Btu/hr ft °F (108)

$\upsilon = k_{air}/k_{fume}$ (109)

$k_{air} = 0.0184$ Btu/hr ft °F (at 212°F) (110)

$p = 0.5$ (porosity of fume) (111)

$k_{comp} = 0.22$ Btu/hr ft °F (112)

$T_o = 114.4°C$ (113)

This is a temperature change of 3.1°C through the deposited fume.

APPENDIX XI. STATISTICAL CALCULATIONS

Calculations to determine the validity of forcing lines through the origin.

See Appendix V: Temperature Effects (this data will be used in the following calculations)

x_i	y_j
0.618	0.618
0.381	0.0431
0.356	0.0367
0.511	0.0365
0	0
0.255	0.0347
0.538	0.0519
0.761	0.0555
0	0
0.253	0.0286
0.446	0.0501
0.456	0.0472
1.130	0.1122
0.135	0.0242
0	0

Using linear regression:

$$y = 0.004074 + 0.08928x \tag{114}$$

$$\bar{x} = 0.389 \tag{115}$$

$$SS_{LOF} = \sum \left(\hat{y}_j - \bar{y}_j \right)^2 = 0.000756 \tag{116}$$

$$SS_{Error} = \sum \left(y_{j,u} - \bar{y}_j \right)^2 = 0 \tag{117}$$

$$SS_{Res} = SS_{LOF} + SS_{Error} = 0.00756 \tag{118}$$

$$DF = 13 \tag{119}$$

$$MS_{Res} = SS_{Res}/DF = 5.818*10^{-5} \tag{120}$$

$$S = \sqrt{MS_{Res}} = 0.007627 \tag{121}$$

$$\sum (x_i - \bar{x})^2 = 1.341 \tag{122}$$

use 95% confidence, $\alpha = 0.05$

$$b_o = \pm t_{0.025,13} S \sqrt{\frac{\sum x_i^2}{n \sum (x_i - \bar{x})^2}} \tag{123}$$

$$t_{0.025,13} = 2.160 \tag{124}$$

$$b_o = \pm 0.00698 \tag{125}$$

This is larger than the y-intercept of 0.004074. Therefore it is valid to force the line through the origin.

Spread of data at $\Delta T / T_w = x_o = 0.5$:

$$S_{\hat{y}_o} = S \sqrt{\frac{1}{n} + \frac{(x_o - \bar{x})^2}{\sum (x_i - \bar{x})^2}} \tag{126}$$

$$= 0.00210 \tag{127}$$

$$y = \hat{y}_o \pm t_{0.025,13} \, S_{\hat{y}_o} \tag{128}$$

$$y = 0.0479 \pm 0.0045 \quad [9.4\%] \tag{129}$$